AN ABSTRACT OF THE THESIS OF

Scott Edward Henderson for the degree of Master of Science in Mathematics presented on June 10, 2008.

Title:

Analysis of Fourth Order Numerical Methods for the Simulation of Electromagnetic Waves in Dispersive Media

Abstract approved: _____

Vrushali Bokil

In this thesis, we investigate the problem of simulating Maxwell's equations in dispersive dielectric media. We begin by explaining the relevance of Maxwell's equations to 21st century problems. We also discuss the previous work on the numerical simulations of Maxwell's equations. Introductions to Maxwell's equations and the Yee finite difference scheme follow. Debye and Lorentz dispersive media are then introduced followed by a description of the use of fourth-order accurate spatial derivative approximations. First we consider using fourth-order spatial methods in free-space and the application of the method to the Debye media problem. The fourth-order Debye method is compared to the Yee Debye method using both stability and phase error analyses. After discussions of Debye media approximations, we consider the application of fourth-order methods to Lorentz media. Four schemes are introduced and are called the JHT, KF, HOJHT and HOKF methods. The stability and phase error properties of the HOJHT and HOKF schemes are defined and are compared to the JHT and KF methods. The KF, HOJHT and HOKF schemes are then compared in simulation and are judged based on max-error and processing time. Out of the four schemes, we find that the HOKF scheme is superior

to the other three schemes for the simulation of electromagnetic waves in Lorentz media. We also find that the fourth-order accurate schemes have specific advantages over the second-order accurate schemes.

Analysis of Fourth Order Numerical Methods for the Simulation of Electromagnetic Waves in Dispersive Media

by

Scott Edward Henderson

A THESIS

submitted to

Oregon State University

in partial fulfillment of
the requirements for the
degree of

Master of Science

Presented June 10, 2008
Commencement June 2009

Master of Science thesis of Scott Edward Henderson presented on June 10, 2008

APPROVED:

Major Professor, representing Mathematics

Chair of the Department of Mathematics

Dean of the Graduate School

I understand that my thesis will become part of the permanent collection of Oregon State University libraries. My signature below authorizes release of my thesis to any reader upon request.

Scott Edward Henderson, Author

ACKNOWLEDGEMENTS

I am very appreciative of the hard work that Dr. Vrushali Bokil has provided during the process of constructing this thesis. Without her guidance, this thesis would not be possible. I would also like to thank Dr. Nathan Gibson for his help with programming in Maple and for serving on my committee. Also, Dr. Malgorzata Peszynska and Dr. Roy Haggerty for being on my committee. On a personal note, I would like to thank my parents and sister for their consistent support.

TABLE OF CONTENTS

TABLE OF CONTENTS (Continued)

LIST OF FIGURES

LIST OF FIGURES (Continued)

LIST OF FIGURES (Continued)

LIST OF TABLES

ANALYSIS OF FOURTH ORDER NUMERICAL METHODS FOR THE SIMULATION OF ELECTROMAGNETIC WAVES IN DISPERSIVE MEDIA

1. INTRODUCTION

Maxwell's equations model the behavior of electromagnetic fields. Although Maxwell's equations were derived in the 1870s [18], the importance of these equations is growing with the advancement of technology. Electromagnetics has applications in military, national security, and health care among others. One of the areas of research since World War II has been the effects of radar. When a radar signal is sent, electromagnetic waves bounce off objects and then are detected back at a receiver. Being able to simulate this numerically allows scientists to test designs for new stealth aircraft. Another tie to defense is the simulation of an electromagnetic pulse, or EMP [18]. In an EMP, a nuclear device is set off above the Earth's atmosphere with a resulting pulse strong enough to burn out electronic equipment below. Using simulations, scientists can determine ways to protect the vital information contained in electronic devices.

A third area that is increasingly becoming intertwined with the study of electromagnetic fields is medicine. Electromagnetic waves passing through cancerous tissue exhibit different behavior than waves passing through normal tissue. R.A. Albanese determines that "a microwave imaging tool can be useful in the assessment of tissue dysfunction and in the detection of cancer" [1]. Once cancer is found, Albanese explains another function of electromagnetic waves. He states that "high peak power fields can transiently open

cell membranes and thus facilitate the entry of chemotherapeutic agents into cancerous tissue" [1]. Using simulations allows different strategies to be tested without the use of human subjects. Another application related to health care is the detection of contaminants underground as well as checking for cracks in pipes carrying dangerous materials [1]. All of these topics show the importance and benefits of numerically simulating Maxwell's equations.

For these simulations, numerical schemes available include finite element and finite difference methods. Finite element methods for Maxwell's equations have been studied in free-space by J-F Lee, R. Lee and A. Cangellaris [7], Monk [9] and R. Lee and A. Cangellaris [8]. Finite element methods have also been used to model dielectric dispersion at low frequrencies by Stoykov et al [15] which includes modeling in both Debye and Lorentz media. Some advantages of finite element methods include the ability to use general meshes and in some cases, unconditional stability [3]. The methods that we consider in this paper are finite difference schemes and are similar in style to the method proposed in 1966 by K. S. Yee [21]. We refer to that scheme as the Yee scheme but it is also known as the Finite Difference Time Domain or "FDTD" method. The Yee scheme is second-order accurate in both time and space or what is referred to as a (2,2) scheme. Prokopidis, Kosmidou, and Tsiboukis propose a FDTD(2,4) scheme for Maxwell's Equations in dispersive media which is referred to as higher-order because it utilizes a fourth-order approximation to the spatial derivative in Maxwell's equations. The main goal of this thesis is to determine whether using fourth-order accurate in space schemes for simulation of Maxwell's Equations in dispersive media is a worthwhile tactic. Along with this, we would like to compare different higher-order schemes to determine if there is a superior fourth-order scheme for the simulation of electromagnetic waves for Lorentz dispersive media.

An outline of the thesis is as follows. Chapter 1 introduces Maxwell's equations and

the Yee finite difference scheme. Also, Chapter 1 discusses Lorentz and Debye dispersive media. Chapter 2 describes the use of fourth-order accurate spatial derivative approximations. First we discuss using this method in free-space and then see its application to the Debye media problem. The fourth-order Debye method is compared to the Yee Debye method using both stability and phase error analyses. In Chapter 3 we discuss using the fourth-order approximation for numerical simulation of EM waves in Lorentz media. Four schemes are introduced and are called the JHT, KF, HOJHT and HOKF methods. The stability and dispersion properties of the HOJHT and HOKF schemes are derived and are compared to the KF and JHT schemes. The KF, HOJHT and HOKF schemes are then compared in numerical simulations of electromagnetic waves in Lorentz media. The schemes are judged based on l_∞-error and processing time. Out of the four schemes, we find that the HOKF scheme is superior to the other three schemes when simulating electromagnetic waves in Lorentz media. We also find that the fourth-order accurate schemes outperform the second-order accurate schemes. We present these conclusions in Chapter 5.

2. MAXWELL'S EQUATIONS AND THE YEE SCHEME IN FREE SPACE AND DISPERSIVE MEDIA

2.1. Maxwell's Equations

Maxwell's equations are a system of hyperbolic partial differential equations that govern the behavior of electromagnetic waves. In free-space, the three-dimensional Maxwell's curl equations are

$$\begin{aligned} \frac{\partial \mathbf{E}}{\partial t} &= \frac{1}{\epsilon_0}\nabla \times \mathbf{H}, \\ \frac{\partial \mathbf{H}}{\partial t} &= -\frac{1}{\mu_0}\nabla \times \mathbf{E}, \end{aligned} \tag{2.1}$$

where $\mathbf{E}$ is the three-dimensional electric field vector, $\mathbf{E} = (E_x, E_y, E_z)$ and $\mathbf{H}$ is the three-dimensional magnetic field vector, $\mathbf{H} = (H_x, H_y, H_z)$ [19]. Also, ϵ_0 is called the free-space permittivity and μ_0 is the free-space permeability. Both ϵ_0 and μ_0 are constants and their values are $8.85418782 \times 10^{-12}$ and $1.25663706 \times 10^{-6}$, respectively. Permittivity is the measure of how well a material stores energy [14]. It is important to note that $\frac{1}{\sqrt{\mu_0 \epsilon_0}} = c$, where c is the speed of light in a vacuum. Recall that the curl of $\mathbf{E}$ is defined as

$$\nabla \times \mathbf{E} = \begin{vmatrix} \vec{x} & \vec{y} & \vec{z} \\ \frac{\partial}{\partial x} & \frac{\partial}{\partial y} & \frac{\partial}{\partial z} \\ E_x & E_y & E_z \end{vmatrix}, \tag{2.2}$$

and

$$\nabla \times \mathbf{H} = \begin{vmatrix} \vec{x} & \vec{y} & \vec{z} \\ \frac{\partial}{\partial x} & \frac{\partial}{\partial y} & \frac{\partial}{\partial z} \\ H_x & H_y & H_z \end{vmatrix} \tag{2.3}$$

is the curl of **H**. Writing this a different way gives us

$$\nabla \times \mathbf{E} = \left(\frac{\partial E_z}{\partial y} - \frac{\partial E_y}{\partial z}\right)\vec{x} + \left(\frac{\partial E_x}{\partial z} - \frac{\partial E_z}{\partial x}\right)\vec{y} + \left(\frac{\partial E_y}{\partial x} - \frac{\partial E_x}{\partial y}\right)\vec{z}, \tag{2.4}$$

and

$$\nabla \times \mathbf{H} = \left(\frac{\partial H_z}{\partial y} - \frac{\partial H_y}{\partial z}\right)\vec{x} + \left(\frac{\partial H_x}{\partial z} - \frac{\partial H_z}{\partial x}\right)\vec{y} + \left(\frac{\partial H_y}{\partial x} - \frac{\partial H_x}{\partial y}\right)\vec{z}. \tag{2.5}$$

We assume that the electric field only oscillates in the (y, z) plane and travels in the z-direction. EM waves are transverse waves, hence they oscillate perpendicularly to the direction of propagation, z. Thus $E_z = H_z = 0$. Also, the electric and magnetic fields travel perpendicularly to one another. With these assumptions, (2.1) reduces to the one-dimensional model

$$\begin{aligned} \frac{\partial H}{\partial t} &= \frac{1}{\mu_0}\frac{\partial E}{\partial z}, \\ \frac{\partial E}{\partial t} &= \frac{1}{\epsilon_0}\frac{\partial H}{\partial z}, \end{aligned} \tag{2.6}$$

with $E(t, z) = E_y(t, z)$ and $H(t, z) = H_x(t, z)$.

2.2. The Yee Scheme

A commonly used method for simulating Maxwell's equations is known as the Yee scheme. It is an explicit finite difference scheme which uses a staggered grid approximation to both the temporal and spatial derivatives. The electric and magnetic fields are staggered in space which means that the discrete version of E has nodes E_j for $j = 0 \ldots N$ and the discrete version of H has nodes $H_{j+1/2}$ for $j = 0 \ldots N - 1$. The Yee scheme in free space

applied to (2.6) is given as:

$$\begin{aligned} \frac{H_{j+1/2}^{n+1/2} - H_{j+1/2}^{n-1/2}}{\Delta t} &= \frac{1}{\mu_0} \frac{E_{j+1}^{n} - E_{j}^{n}}{\Delta}, \\ \frac{E_{j}^{n+1} - E_{j}^{n}}{\Delta t} &= \frac{1}{\epsilon_0} \frac{H_{j+1/2}^{n+1/2} - H_{j-1/2}^{n+1/2}}{\Delta}. \end{aligned} \tag{2.7}$$

We also note that the H and E components are staggered in time with H being computed at $\left(n + \frac{1}{2}\right) \Delta t$ and E computed at $n\Delta t$. In (2.7), Δt is our time step size and Δ is our spatial step size in the z direction. Thus, $E_j^n \equiv E\left(n\Delta t, j\Delta\right)$ and $H_{j+\frac{1}{2}}^{n+\frac{1}{2}} \equiv H\left(\left(n + \frac{1}{2}\right) \Delta t, \left(j + \frac{1}{2}\right) \Delta\right)$. If we solve for $H_{j+1/2}^{n+1/2}$ in the first equation of (2.7) and for E_j^{n+1} in the second we have the following system.

$$H_{j+1/2}^{n+1/2} = H_{j+1/2}^{n-1/2} + \frac{\Delta t}{\mu_0 \Delta} \left(E_{j+1}^{n} - E_{j}^{n}\right) \tag{2.8}$$

$$E_{j}^{n+1} = E_{j}^{n} + \frac{\Delta t}{\epsilon_0 \Delta} \left(H_{j+1/2}^{n+1/2} - H_{j-1/2}^{n+1/2}\right) \tag{2.9}$$

We then use this system to run our simulation. First the system updates the magnetic field in (2.8) and then uses the updated magnetic field values to update the electric field values in (2.9). The computational stencil is shown in Figure 2.1. This shows that the E field at node j at time level $n + 1$ will depend on the H field at nodes $j - \frac{1}{2}$ and $j + \frac{1}{2}$ at time level $n + \frac{1}{2}$ and the previous value of E at node j, i.e., at time level n. This method is second-order accurate in time and space and is conditionally stable for $\nu = \frac{c\Delta t}{\Delta} \leq 1$, where ν is called the Courant number and $\nu \leq 1$ is the Courant-Friedrich-Lewy or CFL condition [16].

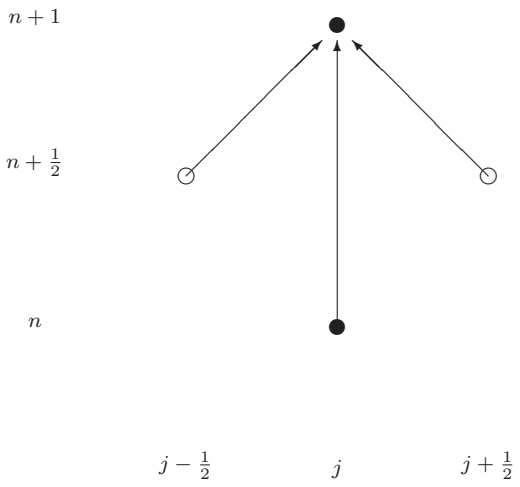

FIGURE 2.1: Computational Stencil for the Yee Scheme shows the updating of the E field [solid circle] at time step n+1 and spatial step j using the value of E at time step n and spatial step j and the values of H [open circle] at j+1/2 and j-1/2 at time step n+1/2

2.3. Dispersive Media

In this thesis, we will discuss numerical methods for Maxwell's Equations in free-space as well as in Debye and Lorentz media. Debye and Lorentz media are two types of dispersive dielectric media. Dielectric media are "such media that do not conduct electricity" [14]. Dispersive refers to the dependence of the media's permittivity on the angular frequency, ω, of the waves passing through it. Angular frequency is defined as $\omega = 2\pi f$ where f is the frequency in Hz [3]. For Debye and Lorentz media, the one-dimensional Maxwell's equations take on the form

$$\begin{aligned} \frac{\partial H}{\partial t} &= \frac{1}{\mu_0}\frac{\partial E}{\partial z}, \\ \frac{\partial D}{\partial t} &= \frac{\partial H}{\partial z}. \end{aligned} \tag{2.10}$$

Note that $\hat{D} = \epsilon(\omega)\hat{E}$ where $\hat{E}$, $\hat{D}$ indicate Fourier transforms of E and D and D is the electric flux density. The dependence of the permittivity ϵ on ω is included in the Yee-scheme by concurrently integrating a differential equation in time that relates D to E [5] or a differential equation in time that expresses the dynamic evolution of the polarization P excited by the propagating electric field [11]. As suggested by Jackson [5] the equation between D and E is derived by taking the inverse Fourier transform of the complex permittivity expression

$$\epsilon(\omega) = \frac{\hat{D}}{\hat{E}}.$$

Using this relation, we rewrite (2.10) as

$$\begin{aligned} \frac{\partial H}{\partial t} &= \frac{1}{\mu_0}\frac{\partial E}{\partial z}, \\ \frac{\partial D}{\partial t} &= \frac{\partial H}{\partial z}, \\ \hat{D} &= \epsilon(\omega)\hat{E}. \end{aligned} \tag{2.11}$$

For Debye media [5],

$$\epsilon(\omega) = \epsilon'_\infty + \frac{\epsilon'_s - \epsilon'_\infty}{1 - i\omega\tau}. \tag{2.12}$$

For Lorentz media

$$\epsilon(\omega) = \epsilon'_\infty - \frac{\omega_0^2(\epsilon'_s - \epsilon'_\infty)}{\omega^2 + 2i\omega\delta - \omega_0^2}. \tag{2.13}$$

In (2.12) and (2.13), $\epsilon'_\infty = \epsilon_\infty\epsilon_0$ and $\epsilon'_s = \epsilon_s\epsilon_0$ where ϵ_∞ is defined as the infinite frequency permittivity and ϵ_s is the static permittivity of the medium. In (2.12), τ is the medium relaxation time and in (2.13), $\delta = \frac{1}{2\tau}$ is the damping coefficient and ω_0 is the medium resonance frequency[11]. We will first discuss numerical simulations of electromagnetic waves in Debye media and then in Lorentz media.

2.3.1 Debye Media

Polarization, in general, is the reaction of the electrons of a medium to electric stimulus [2]. Debye media exhibit *ionic polarization* which means that Debye media are made of materials that form ionic bonds. When an electric field passes through the material, it displaces "atoms or groups of atoms thus creating dipole moments" [14]. In Debye media, the relation between E, the electric field, and D, the electric flux density, is

$$\hat{D} = \epsilon(\omega)\hat{E}, \tag{2.14}$$

where, from (2.12), we have

$$\hat{D} = \left(\epsilon'_\infty + \frac{\epsilon'_s - \epsilon'_\infty}{1 - i\omega\tau}\right)\hat{E}, \tag{2.15}$$

or

$$\hat{D} = \epsilon'_\infty \hat{E} + \frac{\epsilon'_s - \epsilon'_\infty}{1 - i\omega\tau}\hat{E}. \tag{2.16}$$

Multiplying both sides of (2.16) by $1 - i\omega\tau$ we get

$$\begin{aligned}(1 - i\omega\tau)\,\hat{D} &= \epsilon'_\infty \hat{E}\,(1 - i\omega\tau) + \left(\epsilon'_s - \epsilon'_\infty\right)\hat{E} \\ &= \epsilon'_s \hat{E} - i\omega\tau\epsilon'_\infty \hat{E}\end{aligned} \tag{2.17}$$

Transforming to the time domain $\left(-i\omega \to \frac{\partial}{\partial t}\right)$ we get

$$D + \tau\frac{\partial D}{\partial t} = \epsilon'_s E + \epsilon'_\infty \tau\frac{\partial E}{\partial t} \tag{2.18}$$

Collecting the first two equations of (2.11) and equation (2.18) together we get the equations for Debye media, which are

$$\begin{aligned} \frac{\partial H}{\partial t} &= \frac{1}{\mu_0}\frac{\partial E}{\partial z}, \\ \frac{\partial D}{\partial t} &= \frac{\partial H}{\partial z}, \\ D + \tau\frac{\partial D}{\partial t} &= \epsilon'_s E + \epsilon'_\infty \tau \frac{\partial E}{\partial t} \end{aligned} \tag{2.19}$$

Alternatively, if we let $\hat{P} = \frac{\epsilon'_s - \epsilon'_\infty}{1 - i\omega\tau}\hat{E}$ then we have

$$\hat{D} = \epsilon'_\infty E + \hat{P}. \tag{2.20}$$

Multiplying by $-i\omega$ on both sides and transforming to the time domain $\left(-i\omega \rightarrow \frac{\partial}{\partial t}\right)$ transforms (2.20) to

$$\frac{\partial D}{\partial t} = \epsilon'_\infty \frac{\partial E}{\partial t} + \frac{\partial P}{\partial t}. \tag{2.21}$$

In (2.21), P is called the Debye media's macroscopic polarization [14]. Placing (2.21) into (2.11) gives us the following set of equations:

$$\begin{aligned} \frac{\partial H}{\partial t} &= \frac{1}{\mu_0}\frac{\partial E}{\partial z}, \\ \epsilon'_\infty \frac{\partial E}{\partial t} + \frac{\partial P}{\partial t} &= \frac{\partial H}{\partial z}, \\ \hat{P} &= \left(\frac{\epsilon'_s - \epsilon'_\infty}{1 - i\omega\tau}\right)\hat{E}. \end{aligned} \tag{2.22}$$

Multiplying the last equation in (2.22) by $1 - i\omega\tau$ and transforming to the time domain $\left(-i\omega \rightarrow \frac{\partial}{\partial t}\right)$ we get

$$\begin{aligned} \frac{\partial H}{\partial t} &= \frac{1}{\mu_0}\frac{\partial E}{\partial x}, \\ \epsilon'_\infty \frac{\partial E}{\partial t} + \frac{\partial P}{\partial t} &= \frac{\partial H}{\partial z}, \\ P + \tau \frac{\partial P}{\partial t} &= (\epsilon'_s - \epsilon'_\infty)\, E. \end{aligned} \tag{2.23}$$

which are the equations for Debye media in polarization form.

We discretize (2.19) according to the Yee scheme to get:

$$\begin{aligned} H_{j+1/2}^{n+1/2} &= H_{j+1/2}^{n-1/2} + \frac{\Delta t}{\mu_0 \Delta}\left(E_{j+1}^n - E_j^n\right), \\ D_j^{n+1} &= D_j^n + \frac{\Delta t}{\Delta}\left(H_{j+1/2}^{n+1/2} - H_{j-1/2}^{n+1/2}\right), \\ E_j^{n+1} &= \frac{\Delta t + 2\tau}{\eta} D_j^{n+1} + \frac{\Delta t - 2\tau}{\eta} D_j^n + \frac{2\tau\epsilon'_\infty - \epsilon'_s \Delta t}{\eta} E_j^n. \end{aligned} \tag{2.24}$$

where $\eta = 2\tau\epsilon'_\infty + \epsilon'_s \Delta t$ [11]. The last equation is obtained through semi-implicit averaging of both E and D. The scheme (2.24) is second-order accurate in both space and time [11]. The Yee scheme applied to (2.23) results in a numerical method that has identical stability and phase error properties as (2.24), so in this paper we only consider (2.24) for Debye media [11]. It is important to check the stability of this scheme, as the scheme is explicit and hence conditionally stable. Why is stability important? We would like our scheme to better approximate Maxwell's equations as we reduce our spatial and temporal step sizes. This is referred to as a *convergent scheme* [16]. Consistency means that the scheme differs from the partial differential equations pointwise by factors that go to zero as Δ and Δt go to zero. The Lax-Richtmyer Equivalence Relation combines the ideas of stability, consistency and convergence [16].

Theorem 2.3.1.1 (Lax-Richtmyer Equivalence Theorem): *A consistent finite difference scheme for a partial differential equation for which the initial value problem is well-posed*

is convergent if and only if it is stable.

Thus, showing for what conditions our scheme is stable is very important. According to Petropoulos [11], (2.24) has the stability polynomial

$$P_{\text{yee},D}(\chi) = \chi^3 + \gamma_1\chi^2 + \gamma_2\chi + \gamma_3, \tag{2.25}$$

with

$$\gamma_1 = \frac{p^2(h+2) - 6\epsilon_\infty - h\epsilon_s}{2\epsilon_\infty + h\epsilon_s},$$

$$\gamma_2 = \frac{p^2(h-2) + 6\epsilon_\infty - h\epsilon_s}{2\epsilon_\infty + h\epsilon_s},$$

$$\gamma_3 = -\frac{2\epsilon_\infty - h\epsilon_s}{2\epsilon_\infty + h\epsilon_s},$$

with p=$2\nu\rho$, where $\rho = \sin(\frac{k\Delta}{2})$, $h = \frac{\Delta t}{\tau}$, $\nu = \frac{c_\infty \Delta t}{\Delta}$ and k is the wavenumber. The wavenumber is defined as $k = \frac{2\pi}{\lambda}$ where λ is the wavelength. Note that $c_\infty = \frac{c}{\sqrt{\epsilon_\infty}}$ is the fastest speed of propagation in the media while $c_s = \frac{c}{\sqrt{\epsilon_s}}$ is the slowest speed. Also, in free space $\epsilon_\infty = 1$, so $\nu = \frac{c\Delta t}{\Delta}$ as before. In the stability polynomial, χ represents the complex time eigenvalue. The magnitude of χ will determine the stability and numerical dissipation of the scheme. Dissipation is the loss of energy from the propagation of waves as time goes forward. Finding the roots of the stability polynomial and plotting the max root for values of $k\Delta$ between 0 and π will indicate the artificial dissipation of the scheme because "it is known that the FD-TD differenced PDEs should always have $|\chi| = 1$ for all kΔ when ν is less than 1" [11]. Here ν is again the Courant number. We will describe the construction of stability polynomials in detail in Chapters 3 and 4.

Trefethen points out that "there is more to the inaccuracy of a difference scheme than

truncation error" and that errors "caused by differencing are not random perturbations, but a systematic superposition of dispersions and possibly dissipations" [20]. If our system of continuous partial differential equations has solutions of the form $e^{i(kx-\omega t)}$ then there is a corresponding relation between our angular frequency ω and the wavenumber k of the form $\omega = \omega(k)$. This is known as the dispersion relation for the partial differential equations. This means that the wave is propagating at a speed of $\frac{\omega(k)}{k}$. When we use difference methods, we get a different *numerical* dispersion relation and thus a different speed with which waves are travelling in the discrete numerical grid. So even if our numerical scheme has low truncation error, phase error, which is the difference between the phase speed of the differential equations and the numerical scheme, needs to be understood [20]. This is why phase error analysis is important. Petropoulos examines the dispersion of the Yee scheme for Debye media, (2.24), and finds the dispersion relation of the scheme to be [11]

$$k_{\mathrm{num,D}}(\omega\Delta t) = \frac{2}{\Delta}\sin^{-1}\left(\frac{\omega\Delta}{2c}s_\omega\sqrt{\frac{\frac{\epsilon_s}{\tau}\cos\left(\frac{\omega\Delta t}{2}\right) - i\omega s_\omega}{\frac{1}{\tau}\cos\left(\frac{\omega\Delta t}{2}\right) - i\omega s_\omega}}\right), \tag{2.26}$$

where

$$s_\omega = \frac{\sin\left(\frac{\omega\Delta t}{2}\right)}{\frac{\omega\Delta t}{2}}.$$

We can compare this numerical dispersion relation to the dispersion present in the continuous partial differential equations for Debye media i.e., (2.19). The variable $k_{\mathrm{num}} = k_{\mathrm{num,D}}$ is the *numerical wavenumber*, which we want to be close to k, the wavenumber in the differential equations. The dispersion present in the continuous equations (2.19) for Debye media is

$$k_{\mathrm{ex,D}}(\omega) = \frac{\omega}{c}\sqrt{\frac{\frac{\epsilon_s}{\tau} - i\omega}{\frac{1}{\tau} - i\omega}} \tag{2.27}$$

where the ex subscript denotes the "exact" wavenumber [11].

2.3.2 Lorentz Media

Lorentz media have different polarization qualities. When an electric field passes through a Lorentz medium, *electronic polarization* occurs. According to Sihvola, the "phenomenon of electronic polarisation is caused by the displacement of the charge center of the electron cloud with respect to the nucleus [14]. For Lorentz media, we have the following model

$$\begin{aligned} \frac{\partial H}{\partial t} &= \frac{1}{\mu_0}\frac{\partial E}{\partial z}, \\ \frac{\partial D}{\partial t} &= \frac{\partial H}{\partial z}, \\ \hat{D} &= \epsilon(\omega)\hat{E}, \end{aligned} \tag{2.28}$$

where from (2.13)

$$\begin{aligned} \hat{D} &= \left(\epsilon'_\infty - \frac{\omega_0^2(\epsilon'_s - \epsilon'_\infty)}{\omega^2 + 2i\omega\delta - \omega_0^2}\right)\hat{E} \\ &= \epsilon'_\infty \hat{E} + \hat{P}, \end{aligned} \tag{2.29}$$

for

$$\hat{P} = \frac{\omega_0^2(\epsilon'_\infty - \epsilon'_s)}{-\omega^2 + -2i\omega\delta + \omega_0^2}\hat{E}. \tag{2.30}$$

Multiplying both sides by $-\omega^2 - 2i\omega\delta + \omega_0^2$ gives

$$(-\omega^2 - 2i\omega\delta + \omega_0^2)\hat{P} = (\omega_0^2(\epsilon'_\infty - \epsilon'_s))\hat{E}, \tag{2.31}$$

which after transforming to the time domain gives the evolution equation

$$\frac{\partial^2 P}{\partial t^2} + 2\delta\frac{\partial P}{\partial t} + \omega_0^2 P = \omega_0^2(\epsilon'_s - \epsilon'_\infty)E. \tag{2.32}$$

Again, P is called the Lorentz media's macroscopic polarization. With this equation relating E and P, we rewrite (2.28) as

$$\begin{aligned} \frac{\partial H}{\partial t} &= \frac{1}{\mu_0}\frac{\partial E}{\partial z}, \\ \epsilon'_\infty \frac{\partial E}{\partial t} + \frac{\partial P}{\partial t} &= \frac{\partial H}{\partial z}, \\ \frac{\partial^2 P}{\partial t^2} + 2\delta\frac{\partial P}{\partial t} + \omega_0^2 P &= \omega_0^2(\epsilon'_s - \epsilon'_\infty)E. \end{aligned} \tag{2.33}$$

There are two methods that we will discuss for discretizing this set of equations. The two schemes differ in how they discretize $\frac{\partial^2 P}{\partial t^2}$. The first is known as the JHT scheme [5] and it uses a centered second-order discretization for $\frac{\partial^2 P}{\partial t^2}$:

$$\left.\frac{\partial^2 P}{\partial t^2}\right|_j^n \approx \frac{P_j^{n+1} - 2P_j^n + P_j^{n-1}}{\Delta t^2},$$

along with the Yee scheme. This leads to the JHT discretization:

$$\frac{H_{j+1/2}^{n+1/2} - H_{j+1/2}^{n-1/2}}{\Delta t} = \frac{1}{\Delta\mu_0}\left(E_{j+1}^n - E_j^n\right),$$

$$\epsilon'_\infty \frac{E_j^{n+1} - E_j^n}{\Delta t} + \frac{P_j^{n+1} - P_j^n}{\Delta t} = \frac{H_{j+1/2}^{n+1/2} - H_{j-1/2}^{n+1/2}}{\Delta}, \tag{2.34}$$

$$\begin{aligned} \omega_0^2(\epsilon'_s - \epsilon'_\infty)\frac{E_j^{n+1} + E_j^{n-1}}{2} = {} & \frac{P_j^{n+1} - 2P_j^n + P_j^{n-1}}{\Delta t^2} \\ & + 2\delta\left(\frac{P_j^{n+1} - P_j^{n-1}}{2\Delta t}\right) + \omega_0^2\left(\frac{P_j^{n+1} + P_j^{n-1}}{2}\right). \end{aligned}$$

This scheme uses semi-implicit averaging when dealing with E and P in the third equation of (2.34) and a centered first order discretization of the derivative of P. The JHT discretization is second order accurate in both space and time [11]. Petropoulos presents

the JHT stability polynomial [11] in the following way:

$$P_{\mathrm{JHT,Yee}}(\chi) = \chi^4 + \frac{p^2\gamma' + \alpha'}{\eta}\chi^3 + \frac{p^2\theta' + \beta'}{\eta}\chi^2 + \frac{p^2\zeta' + \delta'}{\eta}\chi + \frac{\eta'}{\eta}, \tag{2.35}$$

with

$$\begin{aligned}
\gamma' &= 2 + h_1 + 4\pi^2 h_2^2, \\
\theta' &= -4, \\
\zeta' &= 2 - h_1 + 4\pi^2 h_2^2, \\
\alpha' &= -8\epsilon_\infty - 2h_1\epsilon_\infty - 8\pi^2 h_2^2 \epsilon_s, \\
\beta' &= 12\epsilon_\infty + 8\pi^2 h_2^2 \epsilon_s, \\
\delta' &= -8\epsilon_\infty + 2h_1\epsilon_\infty - 8\pi^2 h_2^2 \epsilon_s, \\
\eta' &= 2\epsilon_\infty - h_1\epsilon_\infty + 4\epsilon_s \pi^2 h_2^2,
\end{aligned}$$

and $\eta = 2\epsilon_\infty + h_1\epsilon_\infty + 4\epsilon_s\pi^2 h_2^2$. In (2.35), $p = 2\nu\rho$ with $\rho = \sin\left(\frac{k\Delta}{2}\right)$.

Petropolous also performs phase error analysis on the JHT scheme. According to Petropolous, the JHT scheme has dispersion relation [11]

$$\rho = \frac{\Delta\omega s_\omega}{2c}\sqrt{\frac{\omega^2 s_\omega^2 \epsilon_\infty - \epsilon_s\omega_0^2\cos(\omega\Delta t) + i\delta\omega\epsilon_\infty s_\omega}{\omega^2 s_\omega^2 - \omega_0^2\cos(\omega\Delta t) + i\delta\omega s_\omega}}, \tag{2.36}$$

where ρ is $\sin\left(\frac{k_{\mathrm{num}}\Delta}{2}\right)$ and $s_\omega = \frac{\sin(\omega\Delta t)}{\frac{\omega\Delta t}{2}}$. Solving this for $k_{\mathrm{num}} = k_{\mathrm{num,JHT}}$ gives

$$k_{\mathrm{num,JHT}}(\omega\Delta t) = \frac{2}{\Delta}\sin^{-1}\left(\frac{\Delta\omega s_\omega}{2c}\sqrt{\frac{\omega^2 s_\omega^2 \epsilon_\infty - \epsilon_s\omega_0^2\cos(\omega\Delta t) + i\delta\omega\epsilon_\infty s_\omega}{\omega^2 s_\omega^2 - \omega_0^2\cos(\omega\Delta t) + i\delta\omega s_\omega}}\right). \tag{2.37}$$

The second scheme for modeling wave propagation in Lorentz media is called the

KF scheme [6] and it treats $\frac{\partial^2 P}{\partial t^2}$ by defining $J = \frac{\partial P}{\partial t}$ and thus $\frac{\partial^2 P}{\partial t^2} = \frac{\partial J}{\partial t}$. This leads to the following first-order system:

$$\begin{aligned} \frac{\partial H}{\partial t} &= \frac{1}{\mu_0}\frac{\partial E}{\partial z}, \\ \epsilon'_\infty \frac{\partial E}{\partial t} + \frac{\partial P}{\partial t} &= \frac{\partial H}{\partial z}, \\ \frac{\partial P}{\partial t} &= J, \\ \frac{\partial J}{\partial t} + 2\delta J + \omega_0^2 P &= \omega_0^2(\epsilon'_s - \epsilon'_\infty)E. \end{aligned} \tag{2.38}$$

Applying the Yee scheme to this formulation gives us the KF scheme:

$$\frac{H_{j+1/2}^{n+1/2} - H_{j+1/2}^{n-1/2}}{\Delta t} = \frac{1}{\Delta \mu_0}\left(E_{j+1}^n - E_j^n\right), \tag{2.39}$$

$$\epsilon'_\infty \frac{E_j^{n+1} - E_j^n}{\Delta t} + \frac{P_j^{n+1} - P_j^n}{\Delta t} = \frac{H_{j+1/2}^{n+1/2} - H_{j-1/2}^{n+1/2}}{\Delta}, \tag{2.40}$$

$$\frac{P_j^{n+1} - P_j^n}{\Delta t} = \frac{J_j^{n+1} + J_j^n}{2}, \tag{2.41}$$

$$\omega_p^2\left(\frac{E_j^{n+1} + E_j^n}{2}\right) = \frac{J_j^{n+1} - J_j^n}{\Delta t} + 2\delta\left(\frac{J_j^{n+1} + J_j^n}{2}\right) + \omega_0^2\left(\frac{P_j^{n+1} + P_j^n}{2}\right). \tag{2.42}$$

In this discretization, semi-implicit averaging is used for the discretization of J in (2.41) as well as for the discretizations of E, P, and J in (2.42). This discretization is also second order accurate in time and space. This scheme has stability polynomial [11]

$$P_{\mathrm{KF,Yee}}(\chi) = \alpha_0\chi^4 + \alpha_1\chi^3 + \alpha_2\chi^2 + \alpha_3\chi + \alpha_4, \tag{2.43}$$

where

$$\begin{aligned}
\alpha_0 &= 2 + \tfrac{2\pi^2 h_2^2 \epsilon_s'}{\epsilon_\infty'} + h_1, \\
\alpha_1 &= \left(h_1 + 2 + 2\pi^2 h_2^2\right) p^2 - 8 - 2h_1, \\
\alpha_2 &= 12 - 4\tfrac{\epsilon_s'}{\epsilon_\infty'}\pi^2 h_2^2 - \left(4 + 4\pi^2 h_2^2\right) p^2, \\
\alpha_3 &= (2 - h_1 + 2\pi^2 h_2^2) p^2 - 8 + 2h_1, \\
\alpha_4 &= -h_1 + 2\pi^2 h_2^2 \tfrac{\epsilon_s'}{\epsilon_\infty'} + 2,
\end{aligned}$$

and ρ is the same as in (2.36).

Petropoulos obtains the following dispersion relation for the KF scheme [11]:

$$\rho = \frac{\omega \Delta s_\omega}{2c} \sqrt{\frac{\omega^2 s_\omega^2 \epsilon_\infty - \epsilon_s \omega_0^2 \cos^2\left(\frac{\omega\Delta t}{2}\right) + 2i\epsilon_\infty \delta \cos\left(\frac{\omega \Delta t}{2}\right) \omega s_\omega}{\omega^2 s_\omega^2 - \omega_0^2 \cos^2\left(\frac{\omega\Delta t}{2}\right) + 2i\delta \cos\left(\frac{\omega\Delta t}{2}\right) \omega s_\omega}}, \tag{2.44}$$

where ρ and s_ω are the same as in (2.36). This gives $k_{\text{num}} = k_{\text{num,KF}}$ for the KF scheme as

$$k_{\text{num,KF}}(\omega \Delta t) = \frac{2}{\Delta} \sin^{-1}\left(\frac{\omega \Delta s_\omega}{2c} \sqrt{\frac{\omega^2 s_\omega^2 \epsilon_\infty - \epsilon_s \omega_0^2 b^2 + 2i\epsilon_\infty \delta b \omega s_\omega}{\omega^2 s_\omega^2 - \omega_0^2 b^2 + 2i\delta b \omega s_\omega}} \right), \tag{2.45}$$

where $b = \cos^2\left(\frac{\omega\Delta t}{2}\right)$. In both the JHT and KF schemes, we will want to compare this dispersion relation with the exact dispersion relation for (2.33) or (2.38) given as [11]

$$k_{ex,L}(\omega) = \frac{\omega}{c} \sqrt{\frac{\omega^2 \epsilon_\infty - \omega_0^2 \epsilon_s + 2i\delta\omega\epsilon_\infty}{\omega^2 - \omega_0^2 + 2i\delta\omega}}, \tag{2.46}$$

which is the dispersion of the partial differential equations for Lorentz media. The KF, JHT and the Debye discretization all utilize a second order approximation to the spatial derivatives as well as a second-order approximation to the temporal derivatives. In the next chapter, we will discuss a fourth order approximation to the spatial derivatives.

3. FOURTH-ORDER ACCURATE SPATIAL APPROXIMATIONS

3.1. Introduction

In the Yee schemes mentioned in Chapter 2, the spatial derivative approximation is second-order accurate. In this chapter, we discuss a fourth-order accurate spatial derivative approximation. The Yee scheme and the new fourth order scheme are both staggered schemes. This means that the spatial derivative at data point $H_{j+1/2}$ uses data points E_j and E_{j+1} in the accompanying spatial derivative. The Yee scheme uses the following approximation for the spatial derivative of E:

$$\left.\frac{\partial E}{\partial z}\right|_{j+1/2} \approx \frac{E_{j+1} - E_j}{\Delta}. \tag{3.1}$$

Since this is a second-order approximation, a reduction of step size Δ by $\frac{1}{2}$ reduces the error between this approximation and the actual derivative by a quarter. Although this scheme is widely used, Yefet and Petropoulos [22] suggest using the following fourth-order approximation for the spatial derivative of E:

$$\left.\frac{\partial E}{\partial z}\right|_{j+1/2} \approx \frac{E_{j-1} - 27E_j + 27E_{j+1} - E_{j+2}}{24\Delta}, \tag{3.2}$$

and the spatial derivative approximation of H:

$$\left.\frac{\partial H}{\partial z}\right|_{j} \approx \frac{H_{j-3/2} - 27H_{j-1/2} + 27H_{j+1/2} - H_{j+3/2}}{24\Delta}. \tag{3.3}$$

In this scheme two electric field points are sampled on each side of our data point $H_{j+1/2}$ and the spatial derivative is fourth-order accurate. This means that a reduction of step

size Δ by $\frac{1}{2}$ results in a reduction of error by a factor of 16. How is this approximation formulated and why is it fourth-order accurate?

Following a method employed in a book by Cohen [4], we will now formulate this approximation. We desire

$$\left.\frac{\partial E}{\partial x}\right|_{j+\frac{1}{2}} + O\left(\Delta^4\right) = AE_{\mathrm{j}+1/2} + a\left(E_{\mathrm{j}+1} - E_j\right) + b\left(E_{\mathrm{j}+2} - E_{\mathrm{j}-1}\right) \tag{3.4}$$

where $O\left(\Delta^4\right)$ means some factor of order 4 in Δ. We use the structure found in (3.4) because we want our staggered scheme to be symmetric about the point $E_{\mathrm{j}+1/2}$. Now $E_{\mathrm{j}+1/2}$ is a fictitious point because we do not actually have that data point. This means that we want A=0 in (3.4). We say that there is a continuous function $E(x)$ such that $E(x)$ has $E(x_{\mathrm{j}+1/2}) = E_{\mathrm{j}+1/2}$ for all of our discrete data points. With this idea in mind, we take Taylor expansions of E_{j}, $E_{\mathrm{j}+1}$, $E_{\mathrm{j}+2}$, and $E_{\mathrm{j}-1}$ centered at the fictitious point $E_{\mathrm{j}+1/2}$. This gives us the following approximations to those points:

$$\begin{aligned} E_{\mathrm{j}+1} \approx\ & E(x_{\mathrm{j}+1/2}) + \frac{\Delta}{2}\frac{\partial E}{\partial x}(x_{j+1/2}) + \frac{\left(\frac{\Delta}{2}\right)^2}{2}\frac{\partial^2 E}{\partial x^2}(x_{j+1/2}) \\ & + \frac{\left(\frac{\Delta}{2}\right)^3}{6}\frac{\partial^3 E}{\partial x^3}(x_{j+1/2}) + O(\Delta^4), \end{aligned} \tag{3.5}$$

$$\begin{aligned} E_{\mathrm{j}} \approx\ & E(x_{\mathrm{j}+1/2}) - \frac{\Delta}{2}\frac{\partial E}{\partial x}(x_{j+1/2}) + \frac{\left(\frac{\Delta}{2}\right)^2}{2}\frac{\partial^2 E}{\partial x^2}(x_{j+1/2}) \\ & - \frac{\left(\frac{\Delta}{2}\right)^3}{6}\frac{\partial^3 E}{\partial x^3}(x_{j+1/2}) + O(\Delta^4), \end{aligned} \tag{3.6}$$

$$\begin{aligned} E_{\mathrm{j}+2} \approx\ & E(x_{\mathrm{j}+1/2}) + \frac{3\Delta}{2}\frac{\partial E}{\partial x}(x_{j+1/2}) + \frac{\left(\frac{3\Delta}{2}\right)^2}{2}\frac{\partial^2 E}{\partial x^2}(x_{j+1/2}) \\ & + \frac{\left(\frac{3\Delta}{2}\right)^3}{6}\frac{\partial^3 E}{\partial x^3}(x_{j+1/2}) + O(\Delta^4), \end{aligned} \tag{3.7}$$

$$E_{\mathrm{j}-1} \approx \; E(x_{\mathrm{j}+1/2}) - \frac{3\Delta}{2}\frac{\partial E}{\partial x}(x_{j+1/2}) + \frac{\left(\frac{3\Delta}{2}\right)^2}{2}\frac{\partial^2 E}{\partial x^2}(x_{j+1/2})$$

$$- \frac{\left(\frac{3\Delta}{2}\right)^3}{6}\frac{\partial^3 E}{\partial x^3}(x_{j+1/2}) + O(\Delta^4). \tag{3.8}$$

Placing (3.5) through (3.8) back into (3.4) we get

$$\left.\frac{\partial E}{\partial x}\right|_{j+1/2} + O\left(\Delta^4\right) = a\left(\Delta\frac{\partial E}{\partial x}(x_{j+1/2}) + \frac{\left(\frac{\Delta}{2}\right)^3}{3}\frac{\partial^3 E}{\partial x^3}(x_{j+1/2})\right) \tag{3.9}$$

$$+b\left(3\Delta\frac{\partial E}{\partial x}(x_{j+1/2}) + \frac{\left(\frac{3\Delta}{2}\right)^3}{3}\frac{\partial^3 E}{\partial x^3}(x_{j+1/2})\right) + O(\Delta^4) \tag{3.10}$$

In order to get the right hand side to look like the left hand side in (3.10), we need

$$a\Delta + 3b\Delta = 1 \tag{3.11}$$

and

$$a\left(\frac{\Delta^3}{24}\right) + b\left(\frac{27\Delta^3}{24}\right) = 0 \tag{3.12}$$

Solving this system gives $b = \frac{-1}{24\Delta}$ and $a = \frac{27}{24\Delta}$ which is (3.2). Since the sides only differ with terms that contain a Δ^4 we can say that these approximations are fourth-order accurate in space. Also, from (3.9) we see that our system is consistent. From the Lax-Richtmyer theorem stated earlier, if we can show stability for this method, we will have convergence.

Another difference between the fourth-order and the second-order approximations is the necessity of changes near the boundary when using the fourth-order scheme. Our electric field approximation consists of points E_j for $j = 0, 1, \ldots, N$ and our magnetic field consists of points $H_{j+1/2}$ for $j = 0, 1, \ldots, N-1$. The second order scheme needs boundary conditions on the electric field nodes of $j = 0$ and $j = N$. In the fourth-order scheme,

our system will try to sample points outside of the domain during the approximations of the temporal derivative at E_0, E_N, E_1, E_{N-1}, $H_{1/2}$ and $H_{N-1/2}$. When we get to those points, our system will try to sample points outside of our domain. We will first discuss the conditions placed at E_0 and E_N, which will be used in both the Yee as well as the fourth order schemes.

3.1.1 Absorbing Boundary Conditions

For our simulations in Chapter 4, we chose to apply first order absorbing boundary conditions at E_0 and E_N. Many of the simulations of Maxwell's equations involve infinite domains. A computer cannot handle infinitely sized domains so absorbing boundary conditions are applied at the boundary nodes so that waves that come to the edge of the simulated domain will leave and not return [17]. How are these absorbing boundary conditions developed?

First, for simplicity, we let our boundary be located in air. This means that as the wave moves toward the boundary, it is propagating at speed c. We can model this by the wave equation. At the node E_0 we set

$$\frac{\partial E}{\partial t} - c\frac{\partial E}{\partial x} = 0, \tag{3.13}$$

and at the node E_N we set

$$\frac{\partial E}{\partial t} + c\frac{\partial E}{\partial x} = 0. \tag{3.14}$$

We will develop the boundary condition for E_0 and the process for developing the boundary condition at E_N will follow the same steps. Although we only have nodes for E at $j = 0, 1, \ldots, N$ and timesteps $n = 0, 1, \ldots, N$ we create fictitious points at half mesh steps and

half time levels for this process. Discretizing (3.13) we get

$$\frac{E_{1/2}^{n+1} - E_{1/2}^{n}}{\Delta t} - c\left(\frac{E_{1}^{n+1/2} - E_{0}^{n+1/2}}{\Delta}\right) = 0. \tag{3.15}$$

Since we don't have any of those four nodes, we use semi-implicit averaging to get (3.15) in terms of E at nodes we have in our system. This leads to

$$\frac{\frac{E_0^{n+1} + E_1^{n+1}}{2} - \frac{E_0^n + E_1^n}{2}}{\Delta t} = c\left(\frac{\frac{E_1^n + E_1^{n+1}}{2} - \frac{E_0^n + E_0^{n+1}}{2}}{\Delta}\right). \tag{3.16}$$

Solving this equation for E_0^{n+1} we get the absorbing boundary condition at E_0 as

$$E_0^{n+1} = E_1^n + \left(\frac{\nu - 1}{\nu + 1}\right)\left(E_1^{n+1} - E_0^n\right). \tag{3.17}$$

3.1.2 One-Sided Approximations

Even with absorbing boundary conditions, this leaves four nodes that require modified approximations in the fourth-order case. Yefet and Petropoulos [22] give these four one-sided approximations in their paper as:

$$\left.\frac{\partial E}{\partial z}\right|_{j=1/2} \approx \frac{-22E_0 + 17E_1 + 9E_2 - 5E_3 + E_4}{24\Delta}, \tag{3.18}$$

$$\left.\frac{\partial E}{\partial z}\right|_{j=N-1/2} \approx \frac{22E_N - 17E_{N-1} - 9E_{N-2} + 5E_{N-3} - E_{N-4}}{24\Delta}, \tag{3.19}$$

$$\left.\frac{\partial H}{\partial z}\right|_{j=1} \approx \frac{-23H_{1/2} + 21H_{3/2} + 3H_{5/2} - H_{7/2}}{24\Delta}, \tag{3.20}$$

$$\left.\frac{\partial H}{\partial z}\right|_{N-1} \approx \frac{23H_{N-1/2} - 21H_{N-3/2} - 3H_{N-5/2} + H_{N-7/2}}{24\Delta}. \tag{3.21}$$

The derivatives of E are both fourth-order accurate and the derivatives of H are third-order accurate. Since the grid is staggered, the scheme is now a $4-3-4-3-4$ accurate scheme [22]. Petropoulos and Yefet describe this as the best boundary treatment. So in free space away from the boundary, we now have the system of equations

$$\begin{aligned}\frac{H_{j+1/2}^{n+1/2}-H_{j+1/2}^{n-1/2}}{\Delta t}&=\frac{1}{\mu_0}\frac{E_{j-1}^{n}-27E_{j}^{n}+27E_{j+1}^{n}-E_{j+2}^{n}}{24\Delta},\\ \frac{E_{j}^{n+1}-E_{j}^{n}}{\Delta t}&=\frac{1}{\epsilon_0}\frac{H_{j-3/2}^{n+1/2}-27H_{j-1/2}^{n+1/2}+27H_{j+1/2}^{n+1/2}-H_{j+3/2}^{n+1/2}}{24\Delta}.\end{aligned} \tag{3.22}$$

The computational stencil for this scheme is shown in Figure 3.1. It shows that the value of E at node j depends on the value of E at the previous time step as well as the values of H at nodes $j-\frac{3}{2},\ j-\frac{1}{2},\ j+\frac{1}{2}$, and $j+\frac{3}{2}$.

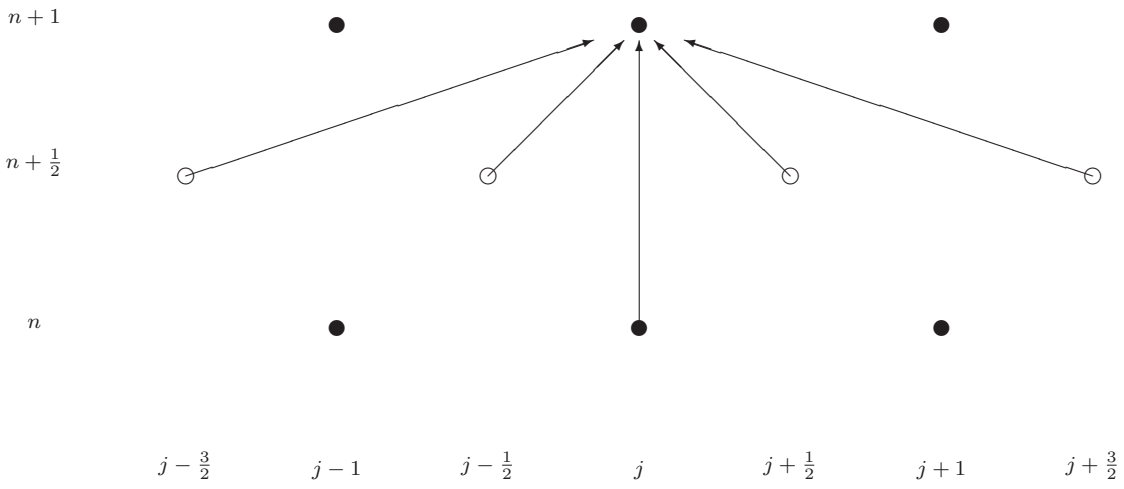

FIGURE 3.1: Computational Stencil for the (2,4) Scheme shows the updating of the E field [solid circle] at spatial node j and time level n+1 using the value of E at node j and time level n and the values of H [open circle] at spatial nodes j-3/2, j-1/2, j+1/2 and j+3/2 at time level n+1/2.

3.2. Stability Analysis in Free Space

Now that we have explained the derivation of the fourth-order scheme, let us discuss what motivated the evolution of this scheme. As we have already stated, the Yee scheme introduces both artificial dispersion and dissipation through its discretization. Using a fourth order scheme, we hope to lessen the impact of these problems. Also, the second-order in space schemes "require that the Courant number $\left[\nu = \frac{c\Delta t}{\Delta}\right]$ used be the maximum allowed for stability (ν=1 in one dimension) in order for them to introduce the least phase error"[12]. This scenario arises when modeling stiff problems where solutions vary rapidly on some interval. Yee scheme approximations introduce substantial amounts of dissipation when ν is reduced from its optimal level. Fourth-order methods allow for a reduction in the value of ν from optimal level without this problem [12]. Now that we have introduced ν, let us check which values of ν result in a stable fourth-order scheme. Plane-wave solutions to the system (3.22) have the form

$$\left\{ \begin{array}{c} H_j^n \\ \\ E_j^n \end{array} \right\} = \left\{ \begin{array}{c} \tilde{h} \\ \\ \tilde{e} \end{array} \right\} \chi^n e^{ikj\Delta}. \tag{3.23}$$

Substituting this into (3.22) gives us the system $A\vec{x} = \vec{0}$ where

$$A = \left[\begin{array}{cc} \chi^{1/2} - \chi^{-1/2} & \frac{-2i\Delta t}{24\mu_0\Delta}\left(27\sin(\frac{k\Delta}{2}) - \sin(\frac{3k\Delta}{2})\right) \\ \frac{-2i\Delta t}{24\epsilon_0\Delta}\left(27\sin(\frac{k\Delta}{2}) - \sin(\frac{3k\Delta}{2})\right) & \chi^{1/2} - \chi^{-1/2} \end{array} \right], \tag{3.24}$$

and $\vec{x} = \left[\tilde{h}, \tilde{e}\right]^T$. Utilizing a triple angle identity, we simplify

$$\begin{aligned}\frac{9}{8}\sin\left(\frac{k\Delta}{2}\right) - \frac{1}{24}\sin\left(\frac{3k\Delta}{2}\right) &= \sin\left(\frac{k\Delta}{2}\right) + \frac{1}{6}\sin^3\left(\frac{k\Delta}{2}\right) \\ &= \sin\left(\frac{k\Delta}{2}\right)\left(1 + \frac{1}{6}\sin^2\left(\frac{k\Delta}{2}\right)\right) \\ &= \rho\left(1 + \frac{\rho^2}{6}\right) = \rho_2\end{aligned} \tag{3.25}$$

for $\rho = \sin\left(\frac{k\Delta}{2}\right)$. Matrix A then becomes

$$A = \begin{bmatrix} \chi^{1/2} - \chi^{-1/2} & \frac{-2i\Delta t\rho_2}{\mu_0\Delta} \\ \frac{-2i\Delta t\rho_2}{\epsilon_0\Delta} & \chi^{1/2} - \chi^{-1/2} \end{bmatrix}. \tag{3.26}$$

The system $A\vec{x} = \vec{0}$ has non-trivial solution if detA=0 which implies that we need

$$(\chi - 2 + \frac{1}{\chi}) + \frac{4\Delta t^2\rho_2^2}{\epsilon_0\mu_0\Delta^2} = 0.$$

If we multiply by $\chi \neq 0$ we have

$$(\chi^2 - 2\chi + 1) + \frac{4\Delta t^2\rho_2^2}{\epsilon_0\mu_0\Delta^2}\chi = 0. \tag{3.27}$$

Utilizing that $\frac{1}{\sqrt{\epsilon_0\mu_0}} = c$ and $\nu = \frac{c\Delta t}{\Delta}$, (3.27) gives us

$$\chi^2 + \chi(4\nu^2\rho_2^2 - 2) + 1 = 0. \tag{3.28}$$

The Routh-Hurwitz stability criterion [10] states that polynomials of the form $\chi^2 + a_1\chi + a_0 = 0$ have roots in the interior of the unit circle iff $-1 + |a_1| < a_0 \leq 1$. In (3.28), $a_0 = 1$

and $a_1 = 4\nu^2\rho_2^2 - 2$, and we have that $|\chi| < 1$ iff $-1 + \left|4\nu^2\rho_2^2 - 2\right| < 1$. This implies that we must have $\nu^2\rho_2^2 < 1$. Since $\rho = \sin\left(\frac{k\Delta}{2}\right)$ and this depends on $k\Delta$, we will need to find the maximum of ρ over all $k\Delta$. Since $|\rho| = \left|\sin\left(\frac{k\Delta}{2}\right)\right| \leq 1$ for all $k\Delta$ and $\rho_2 = \rho\left(1 + \frac{\rho^2}{6}\right)$, we have that

$$\nu^2\rho_2^2 = \frac{\nu^2\rho^2}{36}(6+\rho^2)^2 \leq \frac{49\nu^2}{36}. \tag{3.29}$$

Since we want $|\chi| \leq 1$ for all $k\Delta$ we ask for $\max\limits_{k\Delta} \nu^2\rho_2^2 \leq 1$. From (3.29) $\max\limits_{k\Delta} \nu^2\rho_2^2 = \max\limits_{k\Delta} \frac{\nu^2\rho^2}{36}\left(6+\rho^2\right) = \frac{49\nu^2}{36}$. So $\max\limits_{k\Delta} \nu^2\rho_2^2 \leq 1$ is true if $\frac{49\nu^2}{36} \leq 1$ or $\nu^2 \leq \frac{36}{49} \implies \nu \leq \frac{6}{7}$. Now that we have our stability condition, we are ready to use the fourth-order method for Debye media.

3.3. Fourth Order Method for Debye Media

Replacing the second order accurate spatial derivative approximations in (2.24) by fourth-order approximations gives us the following method for the interior of the domain

$$\begin{aligned}
H_{j+1/2}^{n+1/2} &= H_{j+1/2}^{n-1/2} + \frac{\Delta t}{24\mu_0\Delta}\left(E_{j-1}^n - 27E_j^n + 27E_{j+1}^n - E_{j+2}^n\right), \\
D_j^{n+1} &= D_j^n + \frac{\Delta t}{24\Delta}\left(H_{j-3/2}^{n+1/2} - 27H_{j-1/2}^{n+1/2} + 27H_{j+1/2}^{n+1/2} - H_{j+3/2}^{n+1/2}\right), \\
E_j^{n+1} &= \frac{\Delta t + 2\tau}{\eta}D_j^{n+1} + \frac{\Delta t - 2\tau}{\eta}D_j^n + \frac{2\tau\epsilon'_\infty - \epsilon'_s\Delta t}{\eta}E_j^n,
\end{aligned} \tag{3.30}$$

where $\eta = 2\tau\epsilon'_\infty + \epsilon'_s\Delta t$ [11] along with boundary conditions and the derivative approximations for the points adjacent to the boundary. We note that this system is still second-order accurate in time. We will denote this scheme as a (2,4) scheme.

3.3.1 Stability Analysis

To compare this method to the second order in space scheme, we derive the stability polynomial of (3.30). Again, plane-wave solutions to this set of equations have the form

$$\begin{Bmatrix} H_j^n \\ E_j^n \\ D_j^n \end{Bmatrix} = \begin{Bmatrix} \tilde{h} \\ \tilde{e} \\ \tilde{d} \end{Bmatrix} \chi^n e^{ikj\Delta}. \tag{3.31}$$

Substituting (3.31) into (3.30) we have the system $A\vec{x} = \vec{0}$ where

$$A = \begin{bmatrix} \chi^{1/2} - \chi^{-1/2} & -\frac{2i\Delta t\rho_2}{\mu_0\Delta} & 0 \\ -\frac{2i\Delta t\rho_2}{\Delta} & 0 & \chi^{1/2} - \chi^{-1/2} \\ 0 & \chi - \frac{2\tau\epsilon'_\infty - \epsilon'_s\Delta t}{\eta} & \frac{\Delta t+2\tau}{\eta}\chi + \frac{\Delta t-2\tau}{\eta} \end{bmatrix}, \tag{3.32}$$

and $\vec{x} = \left[\tilde{h}, \tilde{e}, \tilde{d}\right]^T$. In (3.32), ρ_2 is as defined in (3.25). This system has non-trivial solutions when detA=0. So we calculate the determinant of A and set it equal to zero. Through algebraic manipulation we find the stability polynomial of (3.30) to be

$$P_{\mathrm{D,HO}}(\chi) = \chi^3 + \lambda_1\chi^2 + \lambda_2\chi + \lambda_3, \tag{3.33}$$

where

$$\lambda_1 = \frac{p^2(h+2) - 6\epsilon_\infty - h\epsilon_s}{2\epsilon_\infty + h\epsilon_s}, \tag{3.34}$$

$$\lambda_2 = \frac{p^2(h-2) + 6\epsilon_\infty - h\epsilon_s}{2\epsilon_\infty + h\epsilon_s}, \tag{3.35}$$

$$\lambda_3 = -\frac{2\epsilon_\infty - h\epsilon_s}{2\epsilon_\infty + h\epsilon_s}. \tag{3.36}$$

where p=$2\nu\rho_2$, h=$\frac{\Delta t}{\tau}$, $\nu = \frac{c_\infty \Delta t}{\Delta}$.

This stability polynomial has the same structure as (2.25) except for the inclusion of ρ_2 instead of $\rho = \sin\left(\frac{k\Delta}{2}\right)$. Figures 3.2 and 3.3 compare this stability polynomial to the stability polynomial (2.25) for the Yee scheme for values of $k\Delta$ between 0 and π and for values of k between 0 and 8×10^{16}. The wavenumber k is $\frac{2\pi}{\lambda}$ where λ is the wavelength. This means that kΔ is $\dfrac{2\pi\Delta}{\lambda} = \dfrac{2\pi}{\frac{\lambda}{\Delta}}$. So $k\Delta$ is actually $\dfrac{2\pi}{N_w}$ where N_w is the number of points per wavelength [11]. Thus as kΔ is increasing in our graphs, the number of points per wavelength is decreasing.

We use the software MAPLE to plot $\xi = \max|\chi|$ where χ are the roots of the stability polynomial. We plot the maximum because the system will behave according to this eigenvalue. We use the values of $\epsilon_s = 2.25$, $\epsilon_\infty = 1$ and $\tau = 8.1 \times 10^{-12}$ which describe the main relaxation of water in the microwave range of frequencies [11].

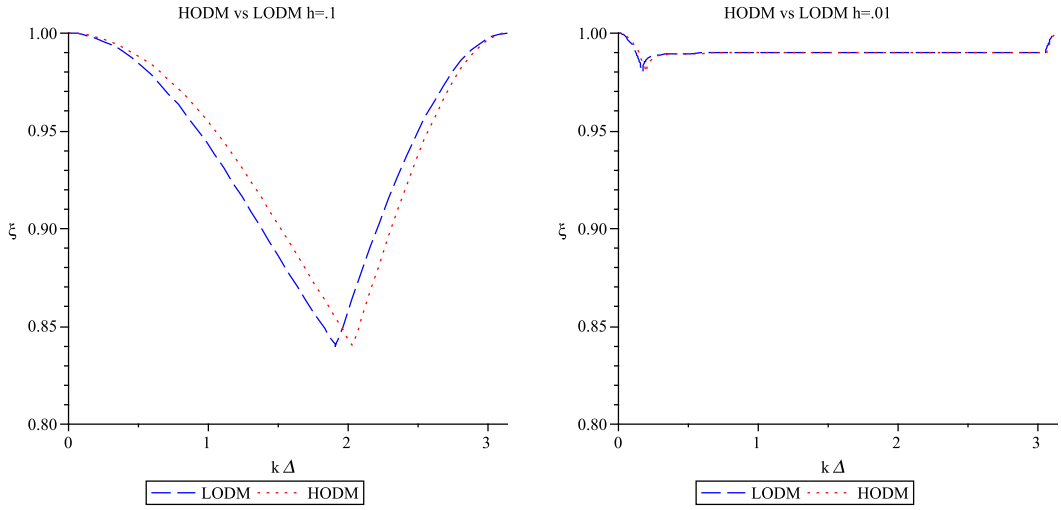

FIGURE 3.2: These plots depict a comparison between the stability of the fourth order debye scheme with the second order Debye scheme for $h = .1$ (left graph) and $h = .01$ (right graph) with independent variable kΔ. In the legend, LODM refers to "lower order" Debye method and HODM refers to "higher order" Debye method.

Figures 3.2 and 3.3 show that the stability polynomial for the (2,4) scheme and the

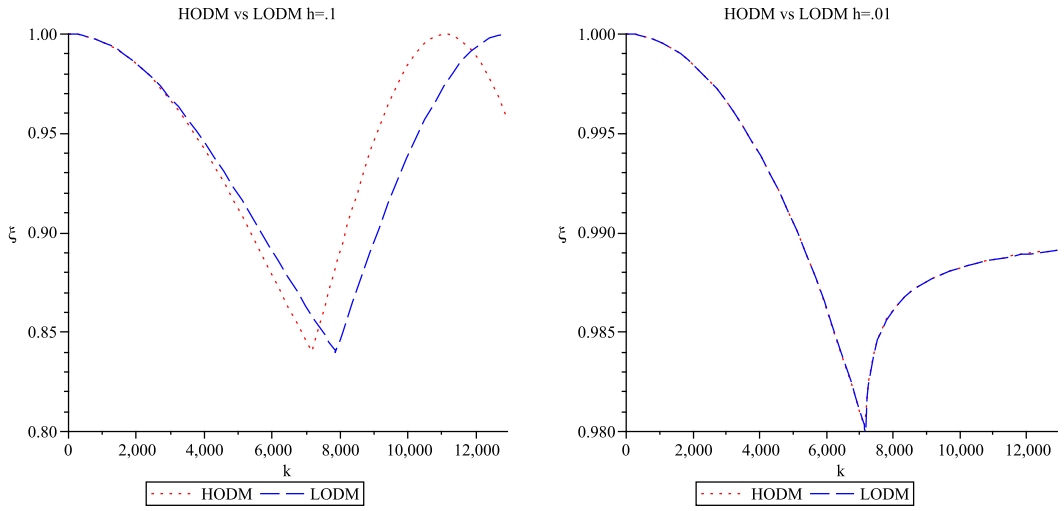

FIGURE 3.3: These plots depict a comparison between the stability of the fourth order Debye media scheme with the second order Debye scheme for $h = .1$ (left graph) and $h = .01$ (right graph) with independent variable k. In the legend, LODM refers to "lower order" Debye method and HODM refers to "higher order" Debye method.

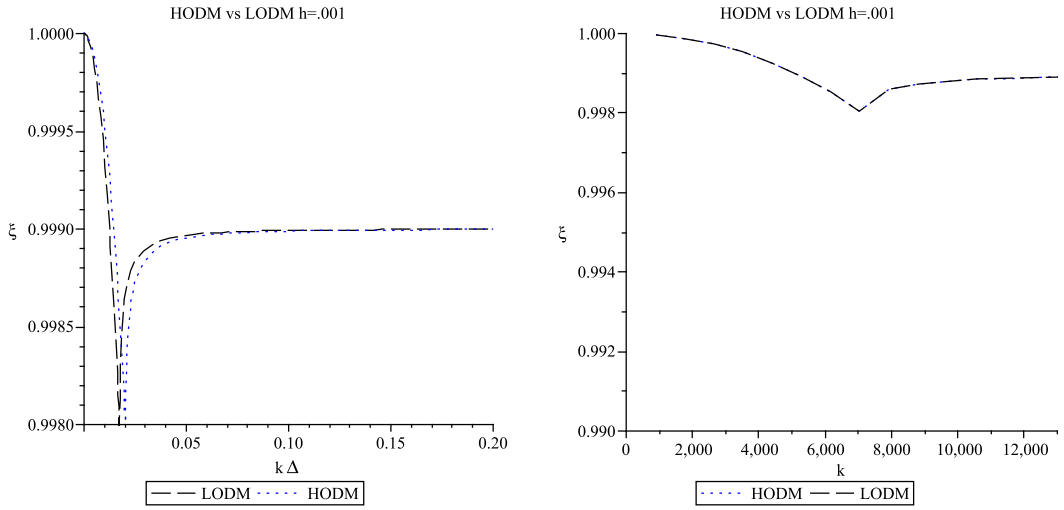

FIGURE 3.4: These plots depict a comparison between the stability of the fourth order Debye media scheme with the second order Debye scheme for $h = .001$ with independent variable kΔ (left graph) and k (right graph). In the legend, LODM refers to "lower order" Debye method and HODM refers to "higher order" Debye method.

Yee scheme exhibit very similar behavior. In the graphs, we call the curves for the (2,4) scheme the HODM or higher-order Debye method and the curves for the (2,2) method the LODM, or lower-order Debye method. We see that for $h = .01$ the curves for the HODM and the LODM are identical at the scale shown. There is still too much dissipation in the scheme with $h = 10^{-2}$ and as Petropoulos concludes for the Yee scheme [11], $\Delta t \approx O\left(10^{-3}\tau\right)$ is needed to control dissipation. Figure 3.4 shows that this requirement of $h = 10^{-3}$ or $\Delta t = O\left(10^{-3}\tau\right)$ seems to also be true for the (2,4) scheme.

3.3.2 Dispersion and Phase Error Analyses

The next test is to check for the phase error in the fourth order numerical scheme and compare it with the phase error in the second-order scheme. To find the numerical dispersion relation of the fourth order Debye method, we substitute

$$\begin{Bmatrix} H_j^n \\ E_j^n \\ D_j^n \end{Bmatrix} = \begin{Bmatrix} \tilde{h} \\ \tilde{e} \\ \tilde{d} \end{Bmatrix} e^{i(k_{\text{num}} j\Delta - \omega n \Delta t)} \tag{3.37}$$

into (3.30) to create the matrix equation $A\vec{x} = \vec{0}$ where

$$A = \begin{bmatrix} -2ia & \frac{-2i\rho_2\Delta t}{\mu_0\Delta} & 0 \\ \frac{-2i\rho_2\Delta t}{\Delta} & 0 & -2ia \\ 0 & -4i\tau\epsilon'_\infty a + 2\epsilon'_s\Delta t b & -2\Delta t b + 4i\tau a \end{bmatrix}, \tag{3.38}$$

with $\vec{x} = \{\tilde{h}, \tilde{e}, \tilde{d}\}^T$ and $\vec{0} = \{0, 0, 0\}^T$. In (3.38), a=$\sin\left(\frac{\omega\Delta}{2}\right)$, and b=$\cos\frac{\omega\Delta t}{2}$. If we let $\epsilon'_\infty = \epsilon_0$ as in the Petropolous paper and simplify, we have the following dispersion

relation:

$$\rho_2 = \frac{\omega\Delta}{2c} s_\omega \sqrt{\frac{\frac{\epsilon_s}{\tau}\cos\left(\frac{\omega\Delta t}{2}\right) - i\omega s_\omega}{\frac{1}{\tau}\cos\left(\frac{\omega\Delta t}{2}\right) - i\omega s_\omega}}, \tag{3.39}$$

where

$$s_\omega = \frac{\sin\left(\frac{\omega\Delta t}{2}\right)}{\frac{\omega\Delta t}{2}}.$$

Again, this only differs from (2.26) by the definitions of ρ and ρ_2. Figures 3.5 and 3.6 show the relation between the phase errors, Φ of the fourth-order scheme and the second-order scheme. Phase error is defined as

$$\Phi = \frac{k_{\text{ex}}(\omega) - k_{\text{num}}(\omega\Delta t)}{k_{\text{ex}}(\omega)}, \tag{3.40}$$

where $k_{\text{ex}}(\omega)$ is defined in (2.27). The phase error compares the dispersion found in the partial differential equations for Debye media with the numerical dispersion found in the (2,4) and (2,2) schemes.

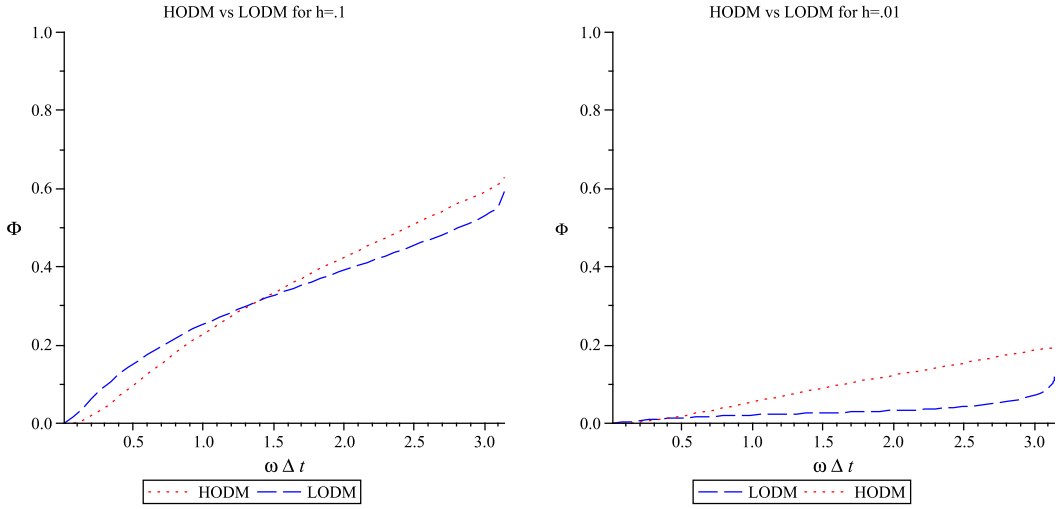

FIGURE 3.5: These plots depict a comparison between the phase error for the fourth order scheme with the second order scheme for $h = .1$ (left graph) and $h = .01$ (right graph) with independent variable $\omega\Delta t$.

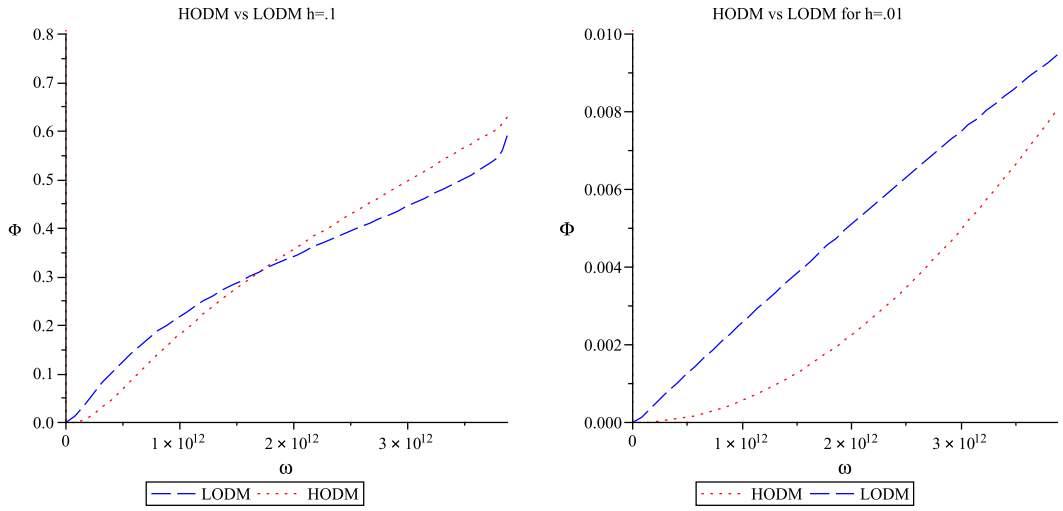

FIGURE 3.6: These plots depict a comparison between the phase error of the fourth order scheme with the second order scheme for $h = .1$ (left graph) and $h = .01$ (right graph) with independent variable ω.

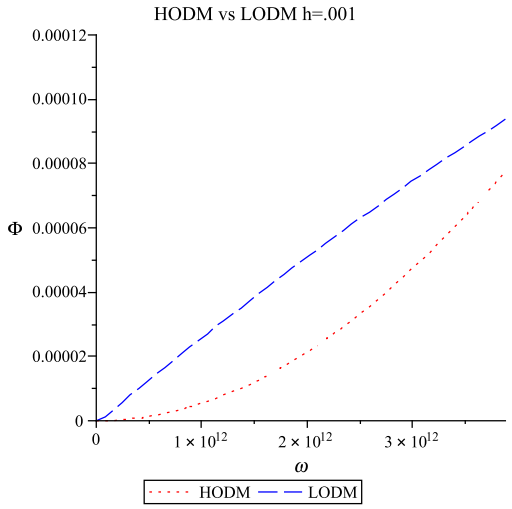

FIGURE 3.7: This plot depicts a comparison between the phase error of the fourth order scheme with the second order scheme for $h = .001$ with independent variable ω.

In Figure 3.5, $\omega\Delta t = \dfrac{2\pi\Delta t}{T} = \dfrac{2\pi}{\frac{T}{\Delta t}} = \dfrac{2\pi}{N_{\mathrm{T}}}$ where T is the period $\left(T = \frac{1}{f}\right)$, where f is frequency and N_{T} is the number of points per period. This means that as our $\omega\Delta t$

increases we have less points per period. In general, we need at least 10 points per period [19]. Figure 3.6 shows that the higher order Debye scheme has less artificial dispersion than the lower order scheme for ω less than approximately 1.5×10^{12} for h=.1 and for all ω shown in the h=.01 graph. Only ω dependence is shown for $h = .001$ because the shift between the HODM and LODM methods obscures the purpose of the graph. Figure 3.7 does show phase error is controlled well at $h = .001$. Thus, we conclude that $\Delta t = O\left(10^{-3}\tau\right)$ gives good stability and dispersion properties for both the (2,2) and (2,4) schemes. Now that we have discussed a fourth-order accurate simulation in Debye media, we will discuss using a fourth order approximation in simulations of Lorentz media in the next chapter.

4. STABILITY AND PHASE ERROR ANALYSES FOR LORENTZ MEDIA METHODS

4.1. Comparison of Numerical Methods for Electromagnetic Wave Propagation in Lorentz Media

In this chapter we will consider the two different formulations for simulating electromagnetic wave propagation in Lorentz media mentioned in Chapter 2. We will compare the KF and JHT schemes to two schemes that use fourth-order approximations for the spatial derivatives. We will refer to these higher-order methods as HOJHT (higher-order JHT) and HOKF (higher-order KF), respectively, according to whether they discretize $\frac{\partial^2 P}{\partial t^2}$ i.e., (2.34) or the first order system corresponding to $P = \frac{\partial J}{\partial t}$, as in (2.39) through (2.42).

4.1.1 Stability Analysis

In this section, we will derive the stability polynomials for the HOKF and HOJHT schemes and compare these polynomials with those obtained from the JHT and KF schemes. We will compare the stability of these four schemes using Fourier stability analysis. Again, we use $\nu=\frac{6}{7}$ as found in Chapter 2 for the higher-order method. This allows us to take the largest temporal step size possible while maintaining stability. As we have already stated, the KF and JHT schemes have optimal $\nu = 1$. So we will be comparing the stabilities of these four methods using each schemes optimal ν.

Replacing the second-order spatial derivatives in (2.39) and (2.40) by fourth-order spatial derivatives we get the following system which we denote as HOKF:

$$\frac{H_{j+1/2}^{n+1/2} - H_{j+1/2}^{n-1/2}}{\Delta t} = \frac{1}{24\Delta\mu_0}\left(E_{j-1}^n - 27E_j^n + 27E_{j+1}^n - E_{j+2}^n\right), \tag{4.1}$$

$$\epsilon'_\infty \frac{E_j^{n+1} - E_j^n}{\Delta t} + \frac{P_j^{n+1} - P_j^n}{\Delta t} = \frac{H_{j-3/2}^{n+1/2} - 27H_{j-1/2}^{n+1/2} + 27H_{j+1/2}^{n+1/2} - H_{j+3/2}^{n+1/2}}{24\Delta}, \tag{4.2}$$

$$\frac{P_j^{n+1} - P_j^n}{\Delta t} = \frac{J_j^{n+1} + J_j^n}{2}, \tag{4.3}$$

$$\omega_p^2 \left(\frac{E_j^{n+1} + E_j^n}{2} \right) = \frac{J_j^{n+1} - J_j^n}{\Delta t} + 2\delta \left(\frac{J_j^{n+1} + J_j^n}{2} \right) + \omega_0^2 \left(\frac{P_j^{n+1} + P_j^n}{2} \right). \tag{4.4}$$

where $\omega_p^2 = \omega_0^2 \left(\epsilon'_s - \epsilon'_\infty \right)$, $\epsilon'_s = \epsilon_0 \epsilon_s$, and $\epsilon'_\infty = \epsilon_0 \epsilon_\infty$. A solution of the HOKF scheme is defined as

$$\begin{Bmatrix} H_j^n \\ E_j^n \\ P_j^n \\ J_j^n \end{Bmatrix} = \begin{Bmatrix} \tilde{h} \\ \tilde{e} \\ \tilde{p} \\ \tilde{j} \end{Bmatrix} \chi^n e^{ikj\Delta}. \tag{4.5}$$

Here we are neglecting the effects of boundary and initial conditions [11]. After this substitution, (4.1) becomes

$$\chi^n e^{ik(j+1/2)\Delta} \left(\chi^{1/2} - \chi^{1/2} \right) \tilde{h} = \frac{\Delta t \chi^n}{24\Delta\mu_0} \left(e^{ik(j-1)\Delta} - 27e^{ik(j)\Delta} + 27e^{ik(j+1)\Delta} - e^{ik(j+2)\Delta} \right) \tilde{e}.$$

Using the fact that $\sin(\theta) = \frac{e^{i\theta} - e^{-i\theta}}{2i}$ and dividing through by $\chi^n e^{ik(j+1/2)\Delta}$ gives us

$$\lambda\tilde{h} - \frac{2i\Delta t}{24\mu_0\Delta} \left(27 \sin\left(\frac{k\Delta}{2} \right) - \sin\left(\frac{3k\Delta}{2} \right) \right) \tilde{e} = 0. \tag{4.6}$$

Likewise, (4.2), (4.3) and (4.4) become

$$\lambda\tilde{e} + \frac{\lambda}{\epsilon'_\infty}\tilde{p} - \frac{2i\Delta t}{24\epsilon'_\infty\Delta} \left(27 \sin\left(\frac{k\Delta}{2} \right) - \sin\left(\frac{3k\Delta}{2} \right) \right) \tilde{h} = 0, \tag{4.7}$$

$$(\kappa - 2)\,\tilde{p} - \frac{\Delta t\,(\kappa)}{2}\tilde{j} = 0, \tag{4.8}$$

$$\omega_p^2 \kappa \tilde{e} - \omega_0^2 \kappa \tilde{p} - \left(\frac{2}{\Delta t}(\kappa - 2) + 2\delta\kappa\right)\tilde{j} = 0 \tag{4.9}$$

respectively. In (4.6) and (4.7), $\lambda = \chi^{1/2} - \chi^{-1/2}$ and in (4.9), $\kappa = \chi + 1$.

We now express (4.6) through (4.9) in the form $A\vec{x} = \vec{0}$ where A is a 4x4 matrix, $\vec{x}$ and $\vec{0}$ are both vectors of length 4. If we define $\vec{x} = \left[\tilde{h}, \tilde{e}, \tilde{p}, \tilde{j}\right]^T$ then we have

$$A = \begin{bmatrix} \lambda & \frac{-2i\Delta t}{\mu_0 \Delta}\rho_2 & 0 & 0 \\ \\ \frac{-2i\Delta t}{\epsilon'_\infty \Delta}\rho_2 & \lambda & \frac{\lambda}{\epsilon'_\infty} & 0 \\ \\ 0 & 0 & \kappa - 2 & \kappa\left(\frac{-\Delta t}{2}\right) \\ \\ 0 & \omega_p^2\kappa & -\omega_0^2\kappa & -\left(\frac{2}{\Delta t}(\kappa - 2) + 2\delta(\kappa)\right) \end{bmatrix}, \tag{4.10}$$

where ρ_2 is as defined in (3.25). This system will only have a nontrivial solution if $det(A) = 0$. Since we are going to be finding the roots of this polynomial, we set the determinant equal to zero and multiply by $-2\Delta t$ without changing our roots. Also, if we assume that $\chi \neq 0$ we can multiply χ through to get a fourth degree polynomial in χ. This gives us the stability polynomial for the HOKF scheme as

$$P_{HOKF}(\chi) = \alpha_0\chi^4 + \alpha_1\chi^3 + \alpha_2\chi^2 + \alpha_3\chi + \alpha_4,$$

with coefficients

$$\alpha_0 = \frac{4\Delta^2\mu_0\epsilon'_\infty + \Delta^2\mu_0\omega_0^2\Delta t^2\epsilon'_s + 4\Delta^2\mu_0\epsilon'_\infty\delta\Delta t}{\epsilon'_\infty\Delta^2\mu_0},$$

$$\alpha_1 = \frac{16\Delta t^3\rho_2^2\delta + 16\Delta t^2\rho_2^2 - 2\Delta^2\mu_0\epsilon'_\infty + 4\Delta t^4\rho_2^2\omega_0^2 - 8\Delta^2\mu_0\epsilon'_\infty\delta\Delta t}{\epsilon'_\infty\Delta^2\mu_0},$$

$$\alpha_2 = \frac{24\Delta^2\mu_0\epsilon'_\infty - 32\Delta t^3\rho_2^2 - 2\Delta^2\mu_0\omega_0^2\Delta t^2\epsilon'_s + 8\Delta t^4\rho_2^2\omega_0^2}{\epsilon'_\infty\Delta^2\mu_0},$$

$$\alpha_3 = \frac{16\Delta t^2\rho_2^2 - 16\Delta t^3\rho_2^2\delta - 16\Delta^2\mu_0\epsilon'_\infty + 8\Delta^2\mu_0\epsilon'_\infty\delta\Delta t + 4\Delta t^4\rho_2^2\omega_0^2}{\epsilon'_\infty\Delta^2\mu_0},$$

$$\alpha_4 = \frac{-4\Delta^2\mu_0\epsilon'_\infty\delta\Delta t + \Delta^2\mu_0\omega_0^2\Delta t^2\epsilon'_s + 4\Delta^2\mu_0\epsilon'_\infty}{\epsilon'_\infty\Delta^2\mu_0}.$$

Our next step is to let $h_1 = \frac{\Delta t}{\tau}$, $h_2 = \frac{\omega_0\Delta t}{2\pi}$, $\delta = \frac{1}{2\tau}$ and to continue to simplify our α's. With these substitutions, the α's become

$$\alpha_0 = 2 + \frac{2\pi^2 h_2^2\epsilon'_s}{\epsilon'_\infty} + h_1,$$

$$\alpha_1 = \left(h_1 + 2 + 2\pi^2 h_2^2\right)p^2 - 8 - 2h_1,$$

$$\alpha_2 = 12 - 4\frac{\epsilon'_s}{\epsilon'_\infty}\pi^2 h_2^2 - \left(4 + 4\pi^2 h_2^2\right)p^2,$$

$$\alpha_3 = (2 - h_1 + 2\pi^2 h_2^2)p^2 - 8 + 2h_1,$$

$$\alpha_4 = -h_1 + 2\pi^2 h_2^2\frac{\epsilon'_s}{\epsilon'_\infty} + 2.$$

where $p = 2\nu\rho_2$. Here ν is $\frac{c_\infty \Delta t}{\Delta}$ and $c_\infty = \frac{1}{\sqrt{\epsilon'_\infty \mu_0}} = \frac{c}{\sqrt{\epsilon_\infty}}$. In the HOKF scheme, $\rho_2 = \frac{1}{24}\left(27\sin\left(\frac{k\Delta}{2}\right) - \sin\left(\frac{3k\Delta}{2}\right)\right)$ as defined in (3.25).

Our main question is how does this compare with the second order KF scheme. As shown in (2.43), the second order KF scheme has the same stability polynomial but with $\rho = \sin\left(\frac{k\Delta}{2}\right)$. In (3.25) we showed

$$\begin{aligned} \rho_2 = \frac{1}{24}\left(27\sin\left(\frac{k\Delta}{2}\right) - \sin\left(\frac{3k\Delta}{2}\right)\right) &= \sin\left(\frac{k\Delta}{2}\right) + \frac{1}{6}\sin^3\left(\frac{k\Delta}{2}\right) \\ &= \rho\left(1 + \frac{\rho^2}{6}\right), \end{aligned} \tag{4.11}$$

and this is the formulation we will be using from here on. How does this change from ρ in the Yee scheme to ρ_2 in HOKF change the behavior of the stability of our new scheme. In Figures 4.1 and 4.2, we compare the results of our HOKF scheme to those found by Petropoulos [11] for the KF scheme. We let $\nu = 1$ for the KF scheme and $\nu = \frac{6}{7}$ for the HOKF scheme. As stated earlier, these are the best CFL conditions for each scheme. For each value of $k\Delta$, where k is the wavenumber, we graph the maximum absolute value of the roots of our stability polynomial, i.e., $\xi = \max|\chi|$. We desire values less than or equal to 1 so that our solution does not grow unbounded as our time steps forward while keeping in mind that values too far from 1 can create unwanted dissipation. As in the Petropoulos paper [11], we use the values $\omega_0 = 4 \times 10^{16}$, $\epsilon'_\infty = \epsilon_0$, $\epsilon_s = 2.25\epsilon_0$, and $\tau = 1.786 \times 10^{-16}$. These are typical values that are used in the study of physical optics and are representative of a highly absorptive and dispersive medium [3].

In Figure 4.1 it is clear that the HOKF plots are very similar to the KF stability plots. Note that in practice we require at least 10 points per period i.e., $k\Delta \leq \frac{2\pi}{10}$ and in this region HOKF has less dissipation. The HOKF plots are shifted a little to the right but have approximately the same shape and also show the same behavior when the spatial

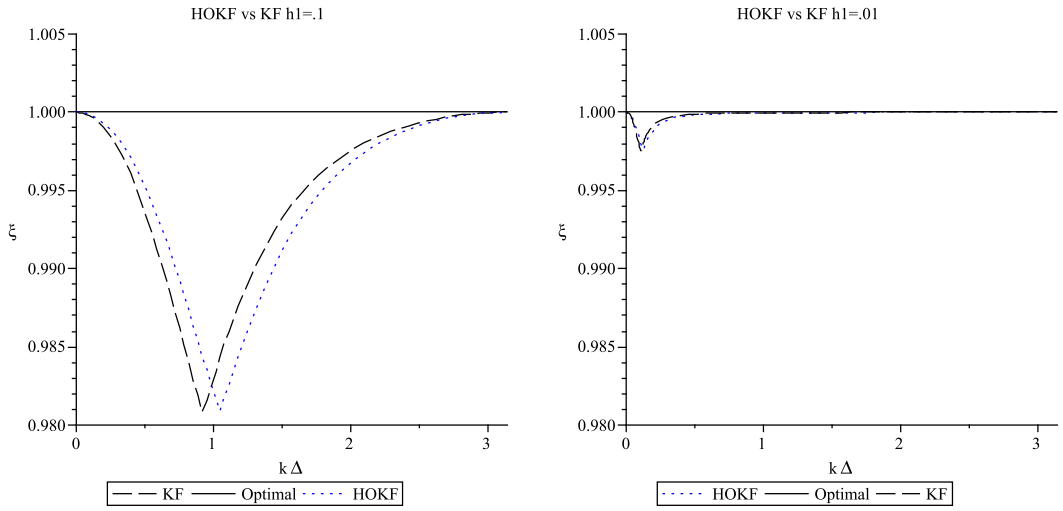

FIGURE 4.1: These plots depict a comparison between the HOKF scheme with the KF scheme for $h_1 = .1$ (left graph) and $h_1 = .01$ (right graph) with independent variable $k\Delta$.

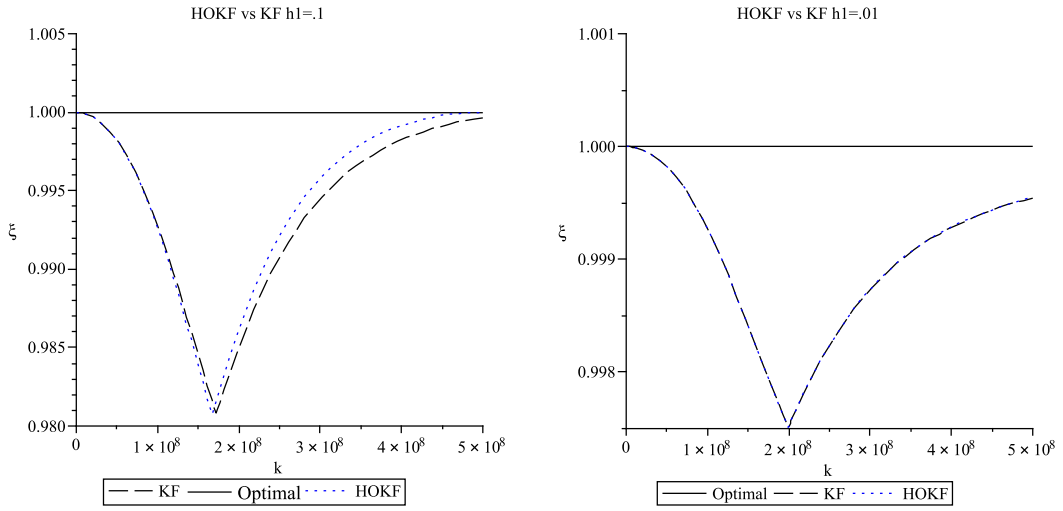

FIGURE 4.2: These plots depict a comparison between the HOKF scheme with the KF scheme for $h_1 = .1$ (left graph) and $h_1 = .01$ (right graph) with independent variable k.

step size is reduced by a factor of 10.

In Figure 4.2, we can see that the stability properties of the two schemes are very comparable but taking away the dependence on Δ takes away much of the shift and allows

us to compare the graph of $h_1 = .1$ and $h_1 = .01$ a little easier. The HOKF scheme is slightly less dissipative at $h_1 = .1$ than the KF scheme. For $h_1 = .01$ the graphs are nearly identical.

We now examine the JHT and HOJHT schemes. Placing the fourth-order accurate approximations into (2.34) gives the following discretization for the HOJHT scheme away from the boundary.

$$\frac{H_{j+1/2}^{n+1/2} - H_{j+1/2}^{n-1/2}}{\Delta t} = \frac{1}{24\Delta\mu_0}\left(E_{j-1}^n - 27E_j^n + 27E_{j+1}^n - E_{j+2}^n\right), \tag{4.12}$$

$$\epsilon'_\infty \frac{E_j^{n+1} - E_j^n}{\Delta t} + \frac{P_j^{n+1} - P_j^n}{\Delta t} = \frac{H_{j-3/2}^{n+1/2} - 27H_{j-1/2}^{n+1/2} + 27H_{j+1/2}^{n+1/2} - H_{j+3/2}^{n+1/2}}{24\Delta}, \tag{4.13}$$

$$\begin{aligned}\omega_0^2(\epsilon'_s - \epsilon'_\infty)\frac{E_j^{n+1} + E_j^n}{2} = & \frac{P_j^{n+1} - 2P_j^n + P_j^{n-1}}{\Delta t^2}, \\ & +2\delta\left(\frac{P_j^{n+1} - P_j^{n-1}}{2\Delta t}\right) + \omega_0^2\left(\frac{P_j^{n+1} + P_j^n}{2}\right).\end{aligned} \tag{4.14}$$

Following a similar procedure as was done for the HOKF scheme above, we have that the stability polynomial for the HOJHT scheme is

$$\chi^4 + \frac{p^2\gamma' + \alpha'}{\eta}\chi^3 + \frac{p^2\theta' + \beta'}{\eta}\chi^2 + \frac{p^2\zeta' + \delta'}{\eta}\chi + \frac{\eta'}{\eta} = 0$$

with

$$\begin{aligned}
\gamma' &= 2 + h_1 + 4\pi^2 h_2^2, \\
\theta' &= -4, \\
\zeta' &= 2 - h_1 + 4\pi^2 h_2^2, \\
\alpha' &= -8\epsilon_\infty - 2h_1\epsilon_\infty - 8\pi^2 h_2^2 \epsilon_s, \\
\beta' &= 12\epsilon_\infty + 8\pi^2 h_2^2 \epsilon_s, \\
\delta' &= -8\epsilon_\infty + 2h_1\epsilon_\infty - 8\pi^2 h_2^2 \epsilon_s, \\
\eta' &= 2\epsilon_\infty - h_1\epsilon_\infty + 4\epsilon_s \pi^2 h_2^2.
\end{aligned}$$

and $\eta = 2\epsilon_\infty + h_1\epsilon_\infty + 4\epsilon_s\pi^2 h_2^2$. Again, $p = 2\nu\rho_2$ where ρ_2 is given in (4.11). In the JHT scheme, as shown by Petropoulos $p = 2\nu \sin\left(\frac{k\Delta}{2}\right) = 2\nu\rho$ [11]. So for both the HOJHT and the HOKF methods, our stability polynomial changes only in the definition of ρ, and hence of p. We used the same values for all constants as in the KF and HOKF plots for the HOJHT and JHT plots in Figures 4.3 and 4.4.

Both in the case where $h_1 = .1$ and $h_1 = .01$ our graphs show very similar behavior. The JHT and HOJHT both become unstable when $h_1 = .1$ but do not when $h_1 = .01$ The JHT scheme becomes unstable at values of $k\Delta$ greater than $\frac{\pi}{2}$ whereas the HOJHT scheme becomes unstable at approximately $k\Delta = 1.64$. As in the HOKF case, the graphs at $h_1 = .01$ become almost indistinguishable. As noted by Petropoulos [11] $h_1 = .01$ seems to be enough to control dissipation in the Yee scheme. This is also true for the HOJHT and the HOKF schemes. Thus $\Delta t \approx O\left(10^{-2}\tau\right)$ is also a requirement for the HOJHT and HOKF schemes.

Now that we have compared the two higher order schemes to their lower order counterparts, we will compare the two higher order schemes. For the next two graphs, we

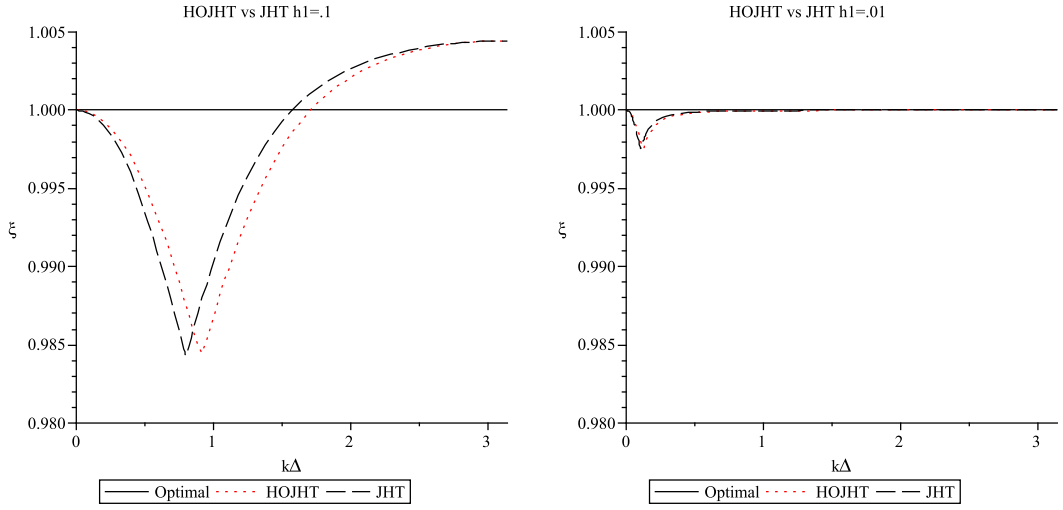

FIGURE 4.3: These plots depict a comparison between the stability of the HOJHT scheme with the JHT scheme for $h_1 = .1$ (left graph) and $h_1 = .01$ (right graph) with independent variable $k\Delta$.

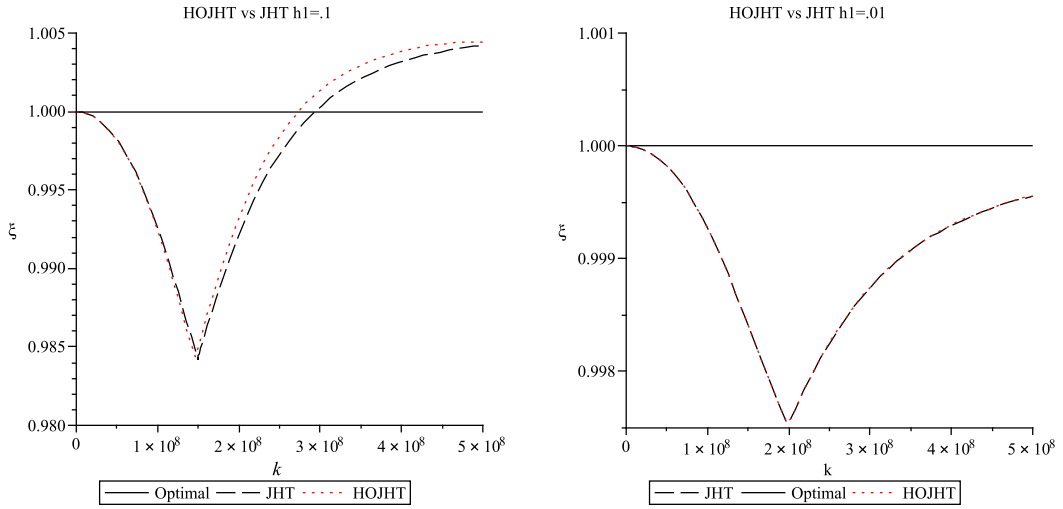

FIGURE 4.4: These plots depict a comparison between the stability of the HOJHT scheme with the JHT scheme for $h_1 = .1$ (left graph) and $h_1 = .01$ (right graph) with independent variable k.

used the same values of constants as before. In Figures 4.5 and 4.6, we can see that the HOKF method does not become unstable when $h_1 = .1$, although it does show a little more dissipation. For $h_1 = .01$ the graphs again are very similar.

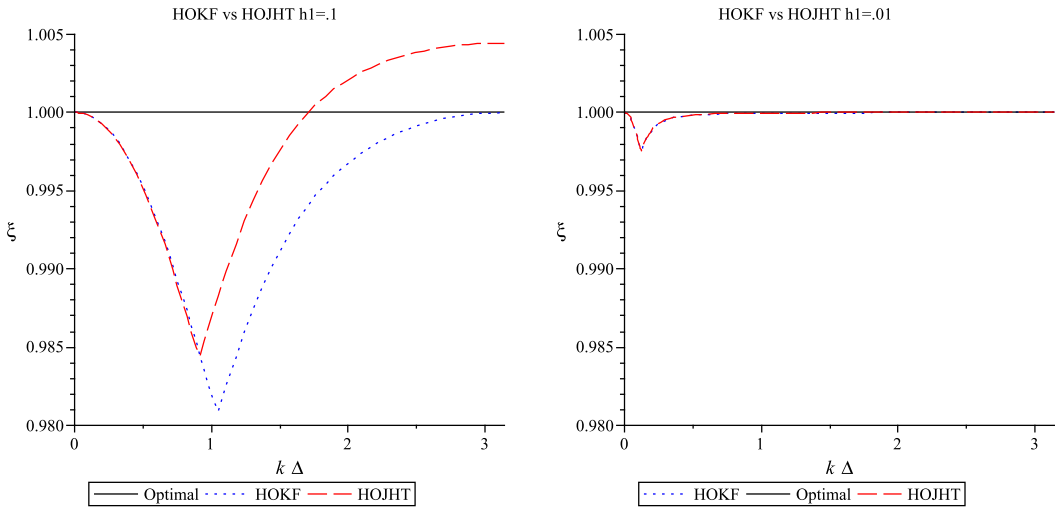

FIGURE 4.5: These plots depict a comparison between the stability of the HOKF scheme with the HOJHT scheme for $h_1 = .1$ (left graph) and $h_1 = .01$ (right graph) with independent variable $k\Delta$.

4.1.2 Dispersion and Phase Error Analysis

In this section, we will derive the numerical dispersion relation for the HOJHT and HOKF schemes and then compare this numerical dispersion to the dispersion present in (2.33) and (2.38) as well as the numerical dispersion in the JHT and KF schemes. The dispersion in the partial differential equations for a Lorentz media was given in (2.46). First, we will go over how to find k_{num} for the HOKF scheme. We again substitute

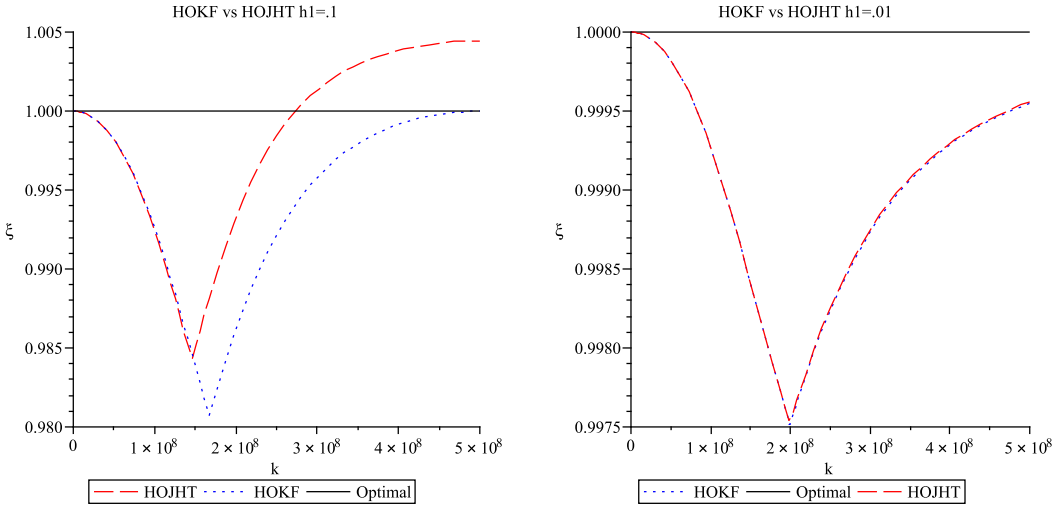

FIGURE 4.6: These plots depict a comparison between the stability of the HOKF scheme with the HOJHT scheme for $h_1 = .1$ (left graph) and $h_1 = .01$ (right graph) with independent variable k.

$$\left\{ \begin{array}{c} H_j^n \\ E_j^n \\ P_j^n \\ J_j^n \end{array} \right\} = \left\{ \begin{array}{c} \tilde{h} \\ \tilde{e} \\ \tilde{p} \\ \tilde{j} \end{array} \right\} e^{i(k_{\text{num}} j\Delta - \omega n \Delta t)}, \tag{4.15}$$

into (4.1)-(4.4). Next, dividing through by $e^{i(k_{\text{num}}(j+1/2)\Delta - \omega n \Delta t)}$ in the equations gives us the four equations

$$C\tilde{h} - \frac{\Delta t}{24\mu_0 \Delta}\left(e^{-i\frac{3k_n\Delta}{2}} - 27e^{-i\frac{k_n\Delta}{2}} + 27e^{i\frac{k_n\Delta}{2}} - e^{i\frac{3k_n\Delta}{2}}\right)\tilde{e} = 0, \tag{4.16}$$

$$\frac{\Delta t}{24\Delta}\left(e^{-i\frac{3k_n\Delta}{2}} - 27e^{-i\frac{k_n\Delta}{2}} + 27e^{i\frac{k_n\Delta}{2}} - e^{i\frac{3k_n\Delta}{2}}\right)\tilde{h} + \epsilon'_\infty C\tilde{e} + C\tilde{p} = 0, \tag{4.17}$$

$$\frac{C}{\Delta t}\tilde{p} - \frac{1}{2}\left(e^{-i\frac{\omega\Delta t}{2}} + e^{i\frac{\omega\Delta t}{2}}\right)\tilde{j} = 0, \tag{4.18}$$

$$\left(\frac{e^{-i\omega\Delta t}-1}{\Delta t}\right)\tilde{j}+\delta\left(e^{-i\omega\Delta t}+1\right)\tilde{j}+\frac{\omega_0^2}{2}\left(e^{-i\omega\Delta t}+1\right)\tilde{p}$$

$$-\frac{\omega_0^2(\epsilon_s'-\epsilon_\infty')}{2}\left(e^{-i\omega\Delta t}-1\right)\tilde{e}=\ 0, \tag{4.19}$$

where $C=\left(e^{-i\frac{\omega\Delta t}{2}}-e^{i\frac{\omega\Delta t}{2}}\right)$. Again we use the fact that $\sin(\theta)=\frac{e^{i\theta}-e^{-i\theta}}{2i}$ and also that $\cos(\theta)=\frac{e^{i\theta}+e^{-i\theta}}{2}$ to simplify our four equations. This gives us that

$$C=-2i\sin\left(\frac{\omega\Delta t}{2}\right),$$

and

$$e^{i\frac{\omega\Delta t}{2}}+e^{-i\frac{\omega\Delta t}{2}}=2\cos\left(\frac{\omega\Delta t}{2}\right).$$

We also have

$$e^{-i\frac{3k_n\Delta}{2}}-27e^{-i\frac{k_n\Delta}{2}}+27e^{i\frac{k_n\Delta}{2}}-e^{i\frac{3k_n\Delta}{2}}=54i\sin\left(\frac{k_{\text{num}}\Delta}{2}\right)-2i\sin\left(\frac{3k_{\text{num}}\Delta}{2}\right).$$

Substituting these identities into (4.16) through (4.19) we get the new set of equations

$$-2i\sin\left(\frac{\omega\Delta t}{2}\right)\tilde{h}-\frac{2i\rho_2\Delta t}{\mu_0\Delta}\tilde{e}=\ 0, \tag{4.20}$$

$$-\frac{2i\rho_2\Delta t}{\Delta}\tilde{h}-2\epsilon_\infty' i\sin\left(\frac{\omega\Delta t}{2}\right)\tilde{e}-2i\sin\left(\frac{\omega\Delta t}{2}\right)\tilde{p}=\ 0, \tag{4.21}$$

$$\frac{-2i}{\Delta t}\sin\left(\frac{\omega\Delta t}{2}\right)\tilde{p}-\cos\left(\frac{\omega\Delta t}{2}\right)\tilde{j}=\ 0, \tag{4.22}$$

$$-\omega_0^2(\epsilon_s'-\epsilon_\infty')\cos\left(\frac{\omega\Delta t}{2}\right)\tilde{e}+\omega_0^2\cos\left(\frac{\omega\Delta t}{2}\right)\tilde{p}+$$

$$\left(\frac{1}{\Delta t}\sin\left(\frac{\omega\Delta t}{2}\right)+2\delta\cos\left(\frac{\omega\Delta t}{2}\right)\right)\tilde{j}=\ 0. \tag{4.23}$$

This leads to a system of equations of the form $A\vec{x}=\vec{0}$ where

$$A=\begin{bmatrix} -2ia & -\frac{2i\rho_2\Delta t}{\mu_0\Delta} & 0 & 0 \\ -\frac{2i\rho_2\Delta t}{\Delta} & -2i\epsilon'_\infty a & -2ia & 0 \\ 0 & 0 & \frac{-2ia}{\Delta t} & -b \\ 0 & -\omega_0^2(\epsilon'_s-\epsilon'_\infty)b & \omega_0^2 b & \frac{1}{\Delta t}a+2\delta b \end{bmatrix}, \tag{4.24}$$

and $\vec{x}=\left[\tilde{h},\tilde{e},\tilde{p},\tilde{j}\right]^T$. In (4.24), $a=\sin\left(\frac{\omega\Delta t}{2}\right)$ and $b=\cos\left(\frac{\omega\Delta t}{2}\right)$. We now take the determinant of A and set it equal to zero. This gives us

$$4(2i\rho_2)^2a^2\Delta t^2-\Delta t^4b^2\omega_0^2(2i\rho_2)^2+4i\Delta t^3\delta ab(2i\rho_2)^2+(4a^2\Delta\sqrt{\epsilon'_\infty\mu_0})^2$$

$$-(2a\omega_0 b\Delta\Delta t\sqrt{\epsilon'_s\mu_0})^2+16i\epsilon'_\infty\delta a^3b\Delta^2\mu_0\Delta t=0.$$

Our goal is to isolate k_{num}, which resides only in ρ_2, so we now collect all groups with $2i\rho_2$ on the left hand side, to get

$$(2i\rho_2)^2(4a^2\Delta t^2-\Delta t^4b^2\omega_0^2+4i\Delta t^3\delta ab)=-(4a^2\Delta\sqrt{\epsilon'_\infty\mu_0})^2$$

$$+(2a\omega_0 b\Delta\Delta t\sqrt{\epsilon'_s\mu_0})^2-16i\epsilon'_\infty\delta a^3b\Delta^2\mu_0\Delta t.$$

This implies that

$$\begin{aligned}(2i\rho_2)^2 =& \frac{-(4a^2\Delta\sqrt{\epsilon'_\infty\mu_0})^2 + (2a\omega_0 b\Delta\Delta t\sqrt{\epsilon'_s\mu_0})^2 - 16i\epsilon'_\infty\delta a^3 b\Delta^2\mu_0\Delta t}{4a^2\Delta t^2 - \Delta t^4 b^2\omega_0^2 + 4i\Delta t^3\delta ab} \\ =& \frac{-4\Delta^2 a^2}{c^2\Delta t^2}\left(\frac{4a^2\epsilon_\infty - \omega_0^2 b^2\Delta t^2\epsilon_s + 4i\epsilon_\infty\delta ab\Delta t}{4a^2 - \Delta t^2 b^2\omega_0^2 + 4i\Delta t\delta ab}\right).\end{aligned} \tag{4.25}$$

Taking the square root of both sides gives us

$$2i\rho_2 = \frac{2i\Delta a}{c\Delta t}\sqrt{\frac{4a^2\epsilon_\infty - \omega_0^2 b^2\Delta t^2\epsilon_s + 4i\epsilon_\infty\delta ab\Delta t}{4a^2 - \Delta t^2 b^2\omega_0^2 + 4i\Delta t\delta ab}}. \tag{4.26}$$

If we let $s_\omega = \frac{2\sin\left(\frac{\omega\Delta t}{2}\right)}{\omega\Delta t}$ our equation simplifies to

$$\rho_2 = \frac{\omega\Delta s_\omega}{2c}\sqrt{\frac{\omega^2 s_\omega^2\epsilon_\infty - \epsilon_s\omega_0^2\cos^2\left(\frac{\omega\Delta t}{2}\right) + 2i\epsilon_\infty\delta\cos\left(\frac{\omega\Delta t}{2}\right)\omega s_\omega}{\omega^2 s_\omega^2 - \omega_0^2\cos^2\left(\frac{\omega\Delta t}{2}\right) + 2i\delta\cos\left(\frac{\omega\Delta t}{2}\right)\omega s_\omega}}. \tag{4.27}$$

Using the definition of ρ_2 in (3.25), our dispersion relation is

$$\rho + \frac{1}{6}\rho^3 = \frac{\omega\Delta s_\omega}{2c}\sqrt{\frac{\omega^2 s_\omega^2\epsilon_\infty - \epsilon_s\omega_0^2\cos^2\left(\frac{\omega\Delta t}{2}\right) + 2i\epsilon_\infty\delta\cos\left(\frac{\omega\Delta t}{2}\right)\omega s_\omega}{\omega^2 s_\omega^2 - \omega_0^2\cos^2\left(\frac{\omega\Delta t}{2}\right) + 2i\delta\cos\left(\frac{\omega\Delta t}{2}\right)\omega s_\omega}}, \tag{4.28}$$

where $\rho = \sin\left(\frac{k_{\text{num}}\Delta}{2}\right)$. Comparing this result for the HOKF to Petropoulos' dispersion relation for the KF scheme [11], we see that it only differs on the left hand side of the equation. How does this affect our phase error? We plot the phase error Φ, (3.40), but with k_{ex} the exact dispersion relation (2.46) for values of $\omega\Delta t$ in $[0, \pi]$ and for values of ω in $\left[0, 8\times 10^{16}\right]$. We use the same values of material parameters in our phase error plots as in our stability plots.

For $h_1 = .1$ in Figure 4.7, we see that for values of $\omega\Delta t$ up to approximately 2 the HOKF scheme has less phase error than the KF scheme. Again, the region $\omega\Delta t < \frac{2\pi}{10}$ is of primary interest in practice. For $h_1 = .01$, the HOKF scheme again outperforms the

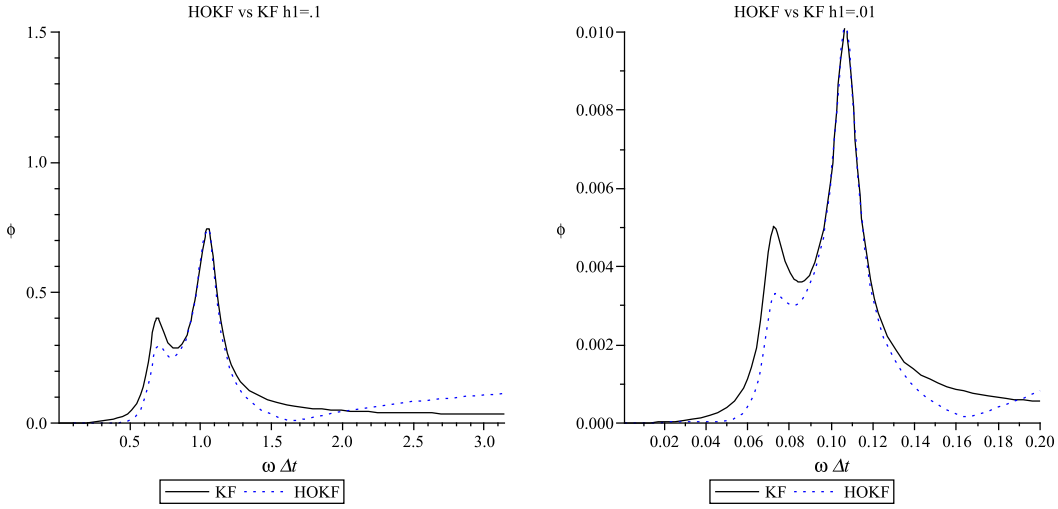

FIGURE 4.7: These plots depict a comparison between the phase error of the HOKF scheme with the KF scheme for $h_1 = .1$ (left graph) and $h_1 = .01$ (right graph) with independent variable $\omega\Delta t$.

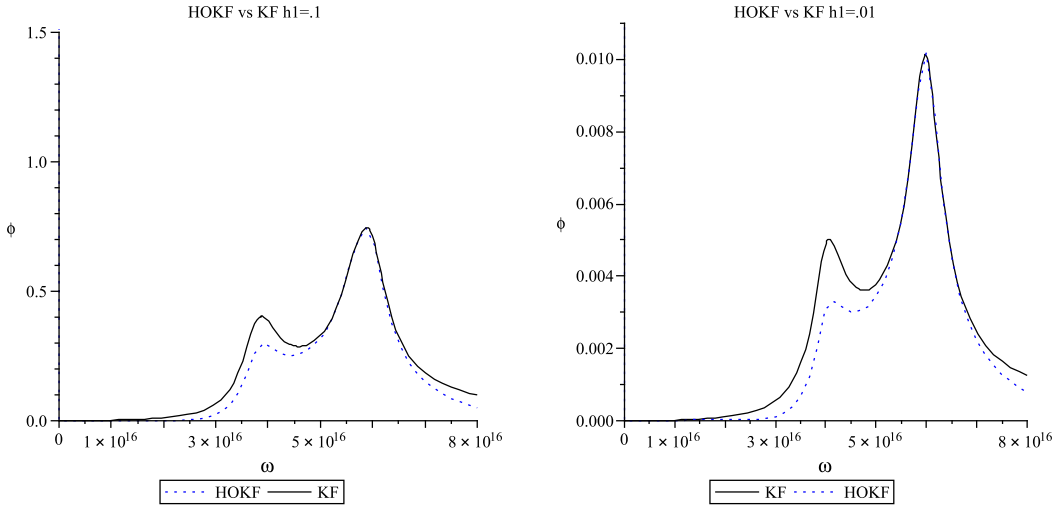

FIGURE 4.8: These plots depict a comparison between the phase error of the HOKF scheme with the KF scheme for $h_1 = .1$ (left graph) and $h_1 = .01$ (right graph) with independent variable ω.

KF scheme for all values of $\omega\Delta t$ up to approximately .19. In Figure 4.8 we see that the HOKF scheme has less phase error than the KF scheme for all values of ω up to 8×10^{16}.

Completing the same analysis for the HOJHT (4.12)-(4.14), we see that the HOJHT method has dispersion relation

$$\sin\left(\frac{k_{\text{num}}\Delta}{2}\right)+\frac{1}{6}\sin^3\left(\frac{k_{\text{num}}\Delta}{2}\right)=\frac{\Delta\omega s_\omega}{2c}\sqrt{\frac{\omega^2 s_\omega^2\epsilon_\infty-\epsilon_s\omega_0^2\cos(\omega\Delta t)+i\delta\omega\epsilon_\infty\frac{\sin(\omega\Delta t)}{\frac{\omega\Delta t}{2}}}{\omega^2 s_\omega^2-\omega_0^2\cos(\omega\Delta t)+i\delta\omega\frac{\sin(\omega\Delta t)}{\frac{\omega\Delta t}{2}}}},$$

which we can compare to the dispersion relation of the JHT scheme given in (2.36). As in the KF and HOKF case, these two dispersion relations only differ on the left hand side of the equation.

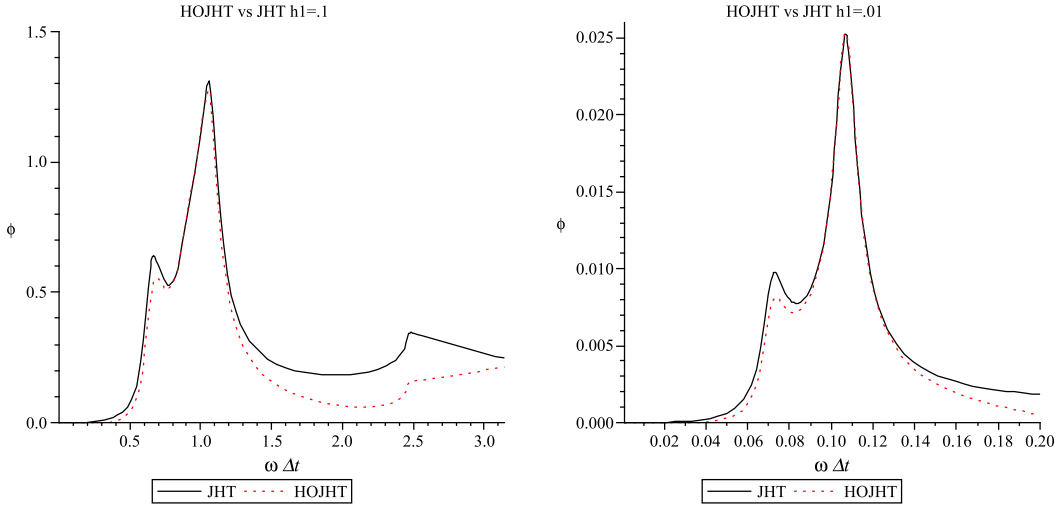

FIGURE 4.9: These plots depict a comparison between the phase error of the HOJHT scheme with the JHT scheme for $h_1 = .1$ (left graph) and $h_1 = .01$ (right graph) with independent variable $\omega\Delta t$.

We compare the phase error for the JHT and HOJHT schemes in Figure 4.9 and Figure 4.10. In these plots we see that for both $h_1 = .1$ and $h_1 = .01$ the HOJHT method outperforms the JHT method for all values of $\omega\Delta t$ in Figure 4.9 and for all values of ω in Figure 4.10.

Now that we have compared the fourth order schemes to their second order counter-

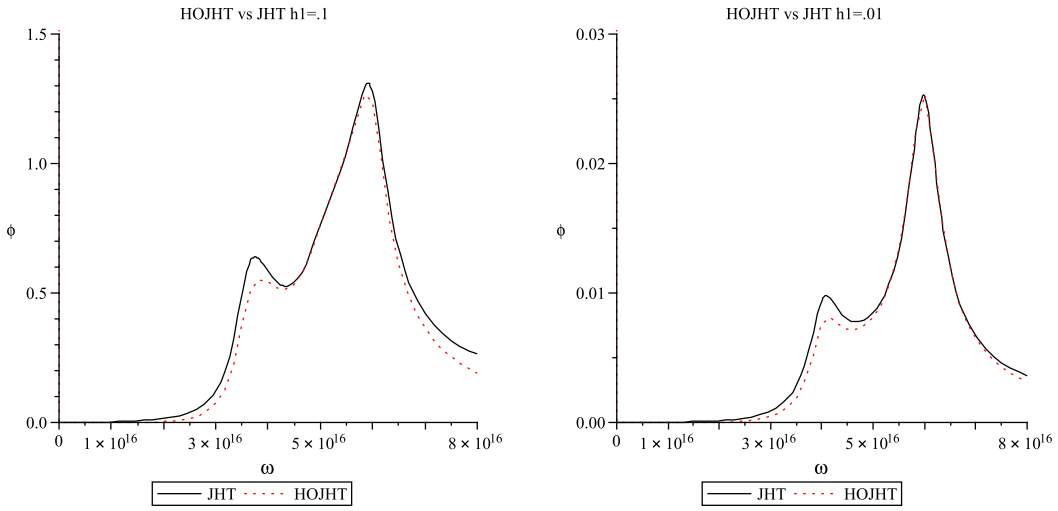

FIGURE 4.10: These plots depict a comparison between the phase error of the HOJHT scheme with the JHT scheme for $h_1 = .1$ (left graph) and $h_1 = .01$ (right graph) with independent variable ω.

parts, we compare the phase error in the HOKF scheme to the phase error in the HOJHT scheme. In Figures 4.11 and 4.12, we compare plots of the phase error for the HOKF scheme and the HOJHT scheme.

The HOKF method far outperforms the HOJHT method for all values of $\omega\Delta t$ from 0 to π in Figure 4.11 and for all values of ω from 0 to 8×10^{16} in Figure 4.12. Note that HOKF requires only slightly more computational effort than HOJHT, as demonstrated in Table 4.2.

4.2. Simulations

In this section, we will be discussing three different simulations. The goal of the first simulation is to show the rate of convergence for the HOKF scheme. For this simulation, the pulse is placed in the center of a Lorentz medium. There are no air to Lorentz

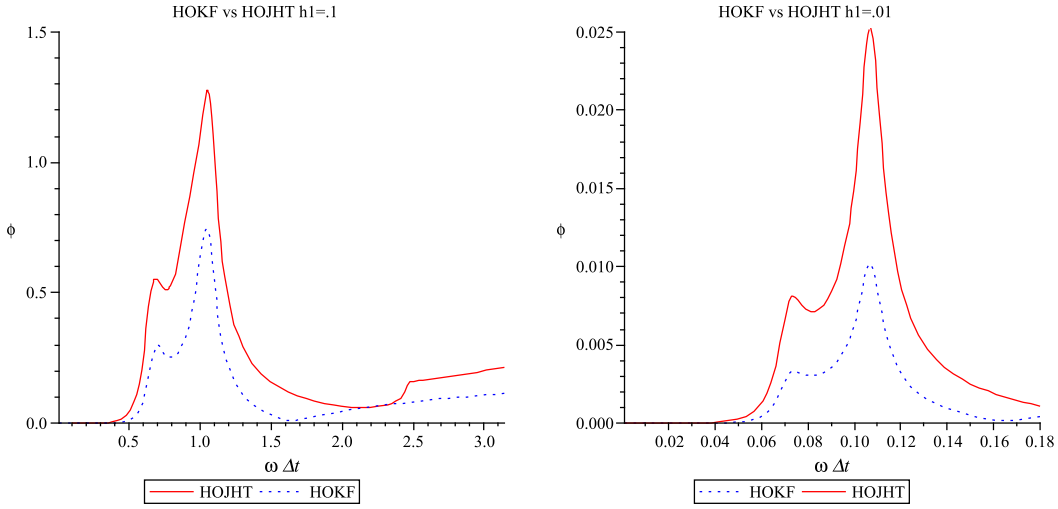

FIGURE 4.11: These plots depict a comparison between the phase error of the HOKF scheme with the HOJHT scheme for $h_1 = .1$ (left graph) and $h_1 = .01$ (right graph) with independent variable $\omega\Delta t$.

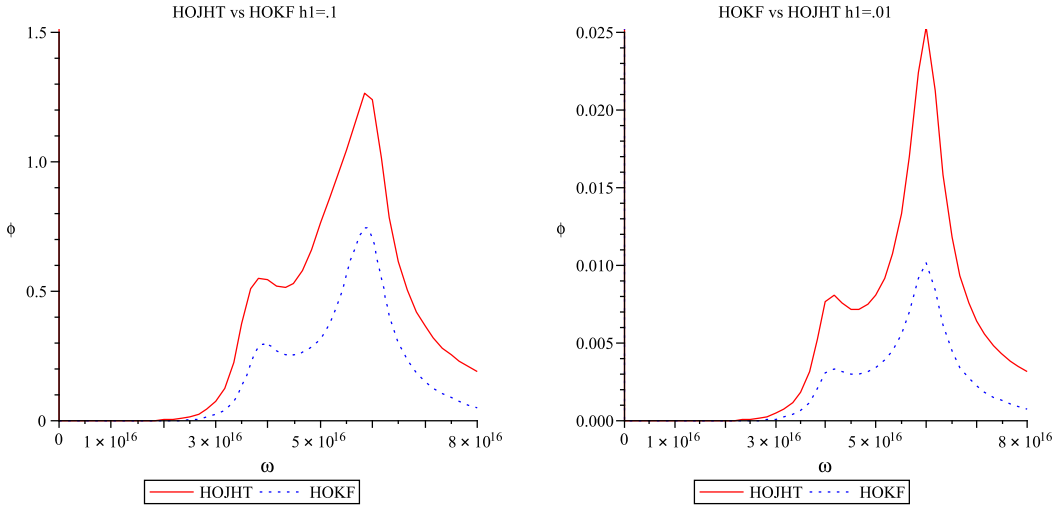

FIGURE 4.12: These plots depict a comparison between the phase error of the HOKF scheme with the HOJHT scheme for $h_1 = .1$ (left graph) and $h_1 = .01$ (right graph) with independent variable ω.

interfaces in the domain and the pulse does not reach the boundary so we can ignore the effects of boundary and interface conditions [a simple reflecting boundary condition i.e.,

$E_0 = 0.0$ and $E_N = 0.0$ are used at the boundary [19]] . Since the temporal derivative approximation is second-order accurate, in order to test for fourth order convergence, we reduce the time step by $\frac{1}{4}$ when we reduce the spatial step by $\frac{1}{2}$. Three solutions are computed using the HOKF method and are plotted at time 8×10^{-14} in Figure 4.13. The

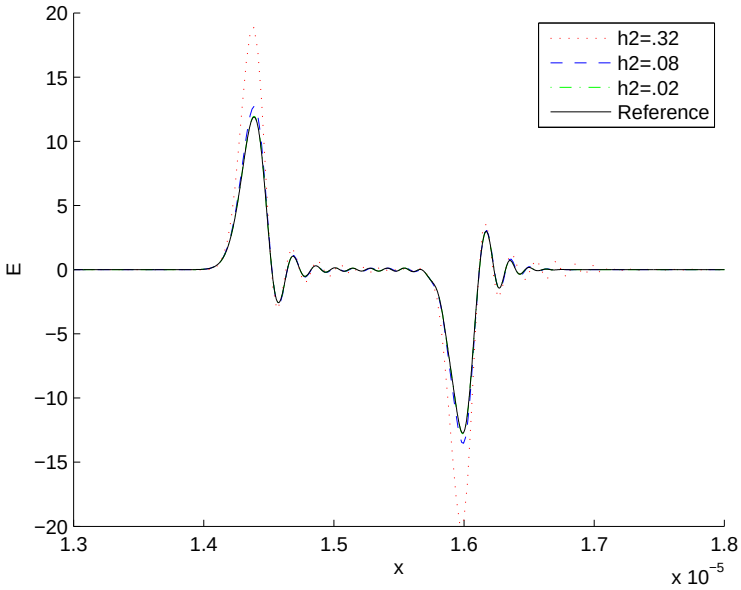

FIGURE 4.13: This graph shows the plots of the three computed solutions as well as the reference solution at time 8×10^{-14}.

errors are calculated using l_2 grid norm error,

$$Error_\Delta = \sqrt{\Delta} \left(\sum_{j=1}^{M} (C_\Delta(j) - Ref(j))^2 \right)^{\frac{1}{2}}$$

where Ref is the reference solution with $\Delta = 1.825 \times 10^{-9}$ and $\Delta t = 1.9 \times 10^{-19}$. The reference solution is restricted to the nodes $1 \ldots M$, where M is the number of nodes in the computed solution C_Δ. The rates are found by comparing the errors of the computed

Δ	Δt	ν	h_2	Error	Rate
2.92e-8	4.88e-17	$\frac{1}{2}$	.32	.0055	
1.46e-8	1.22e-17	$\frac{1}{4}$	.08	.000654	3.073
7.3e-9	3.05e-18	$\frac{1}{8}$	.02	4.58e-5	3.834

TABLE 4.1: The table shows the ratios between the logarithm of the errors for $h_2 =$ .32, .08, and .02.

solutions in the following manner:

$$Rate_{\Delta} = \frac{\log\left(\frac{Error_{2\Delta}}{Error_{\Delta}}\right)}{\log(2)}$$

The errors as well as the rates are shown in Table 4.1. As the grid is refined, the rate seems to be converging to 4, which is expected in a fourth-order accurate scheme.

The second simulation is to check for convergence of the HOKF and HOJHT methods. This simulation was adapted from a paper by Banks, Bokil and Gibson[2]. For each method, we begin the pulse shown in (4.14) in air and let it travel through a slab of Lorentz media before exiting into air on the other end. We use absorbing boundary conditions and one-sided approximations as discussed in Chapter 3. We record the value of the electric field at a point within the Lorentz slab which is at a depth of .01m into the Lorentz material. We refine our grid by reducing the value of $h_2 = .08, .04, .02, .01$ where $h_2 = \frac{\omega_0 \Delta t}{2\pi}$ as in the stability polynomials for the four Lorentz schemes. For both the HOKF and the HOJHT schemes, we let $\nu = \frac{1}{2}$. With this choice of ν we can show that the schemes converge for even small values of ν. For this simulation we chose to test for convergence with h_2 instead of h_1 because of the values for $\epsilon_s, \epsilon_\infty, \tau$, and ω_0 in the problem. With the choices of constants in this simulation, h_2 is smaller than h_1 and one

always wants to resolve the smallest timescale in the problem. In the stability and phase error, we varied h_1 instead of h_2 in order to compare our results with Petropoulos [11].

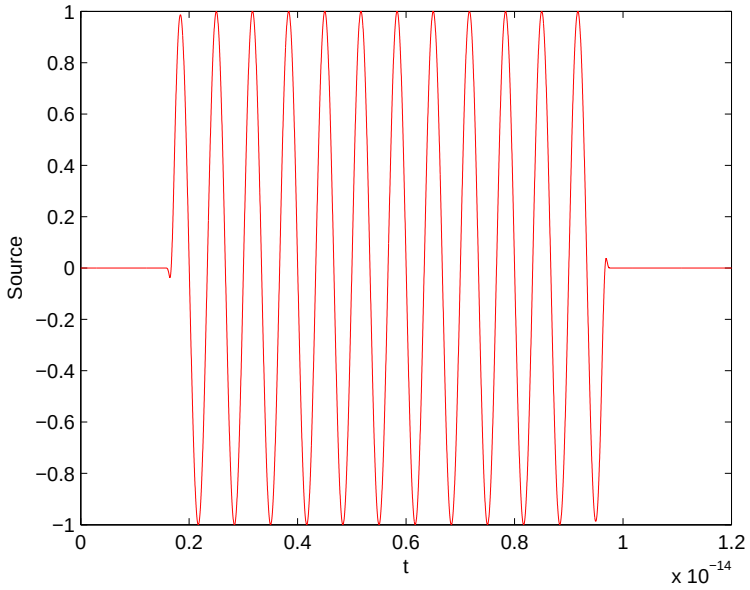

FIGURE 4.14: This is the pulse for the first simulation.

In Figures 4.15 and 4.19 we see that both the HOKF and HOJHT schemes are converging to the same solution curve and Figures 4.16 and 4.20 add more evidence to this claim. At this scale, it is hard to tell the difference between the two schemes. For this reason, we decided to zoom in on two of the center curves. Figures 4.17, 4.21, 4.18, and 4.22 show fairly large amounts of dissipation and artificial dispersion for $h_2 = .08$ but as we refine the grid to $h_2 = .01$ we see that our solution curves are converging. The disparity between the curves for $h_2 = .02$ and $h_2 = .01$ is very small compared to the difference between the curves for $h_2 = .04$ and $h_2 = .02$. Figures 4.21 and 4.22 show that the HOJHT scheme has slightly worse dissipation for larger h_2 and seems to converge slower.

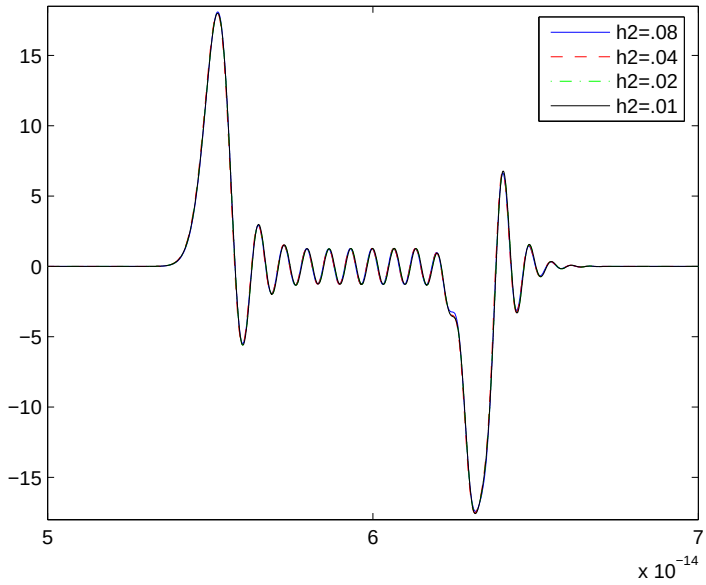

FIGURE 4.15: This plot shows the convergence of HOKF.

The third simulation is adapted from a paper by Prokopidis [13]. For this simulation, we again start a pulse in air and let it pass through a Lorentz medium. Absorbing boundary conditions and one-sided approximations are used as in simulation 1. The pulse is shown in Figure (4.23). The curves for the four schemes are plotted along with a very refined approximation in Figure 4.24 (Exact).

In this simulation, we tested the errors of the four schemes for small values of ν using an l_∞-error. As stated earlier, one advantage of the higher-order methods is their ability to use values less than their optimal ν with less increase in artificial dissipation. The Yee scheme is tested at values of $\Delta = .01$ and $\Delta = .05$ with $\nu = .5$ while the HOKF and HOJHT scheme are tested at values of $\Delta = .05$ and $\nu = .1$. The values of ν were chosen to ensure that Δt is the same in all schemes.

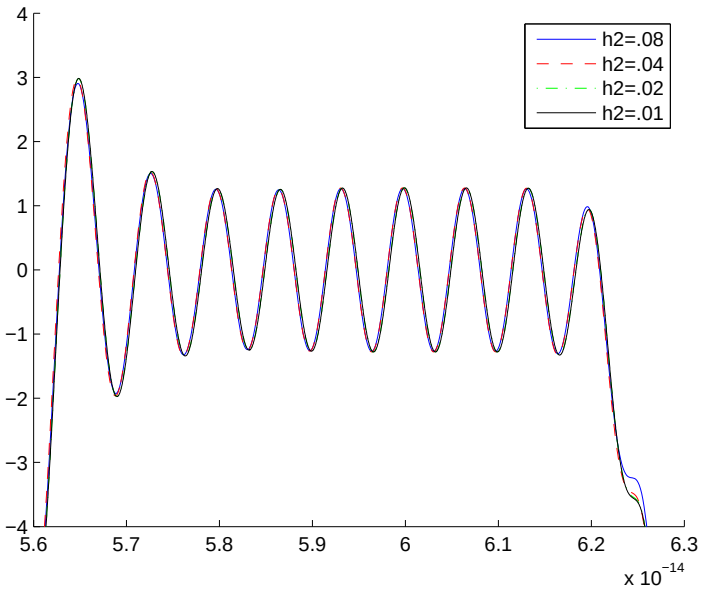

FIGURE 4.16: This plot shows the convergence of HOKF. We have zoomed in on the center of the curve for more detail.

Scheme	ν	Δ	Error	Time
HOKF	.1	.05	.0766	2.51
HOJHT	.1	.05	.0766	2.32
Yee	.5	.05	.3564	.32
Yee	.5	.01	.0828	9.436

TABLE 4.2: Shows the errors and run times for the KF, HOKF, and HOJHT schemes.

The error in the table is calculated as

$$\frac{\max_{j=1}^{N} |C(j) - Ref(j)|}{\max_{j=1}^{N} |Ref(j)|}$$

where Ref is the reference solution restricted to the nodes of C, which corresponds to one of the methods used in the simulation. As seen in the table, even with five times as many

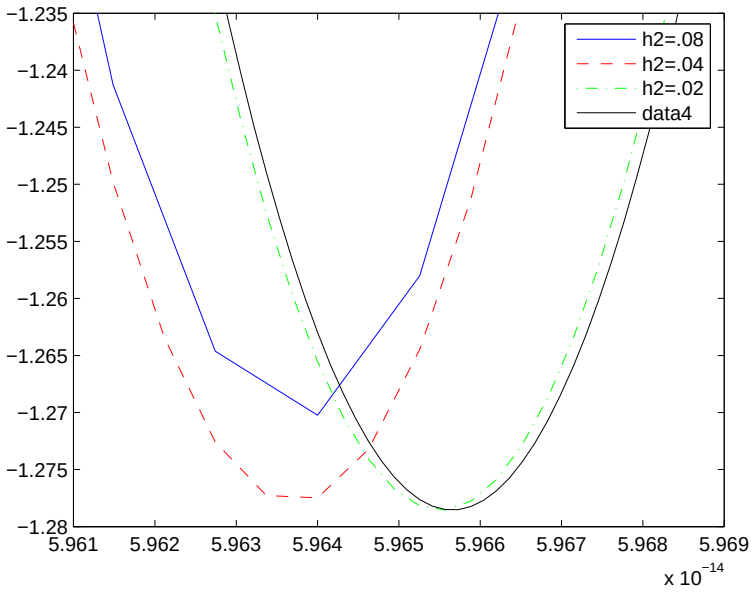

FIGURE 4.17: This plot shows the convergence of HOKF. We have zoomed in on one of the center curves for more detail.

nodes the Yee scheme is still outperformed by the two higher-order methods. The HOKF and HOJHT methods exhibit very similar behavior. This is due to the simulation having a h_2 value less than .01. This downplays any differences between the two higher-order schemes.

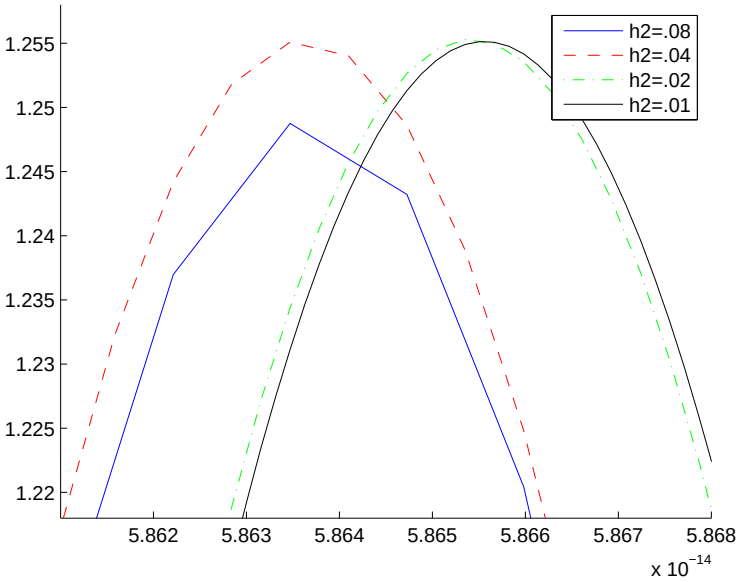

FIGURE 4.18: This plot shows the convergence of HOKF. We have zoomed in on one of the center curves for more detail.

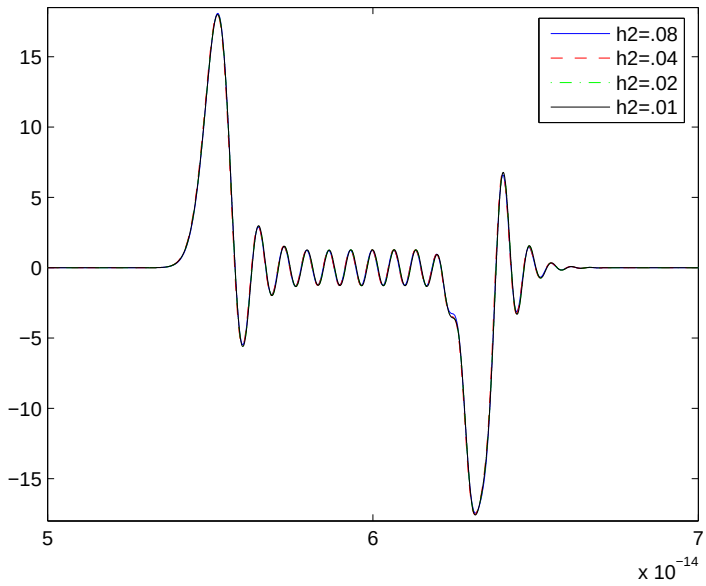

FIGURE 4.19: This plot shows the convergence of HOJHT.

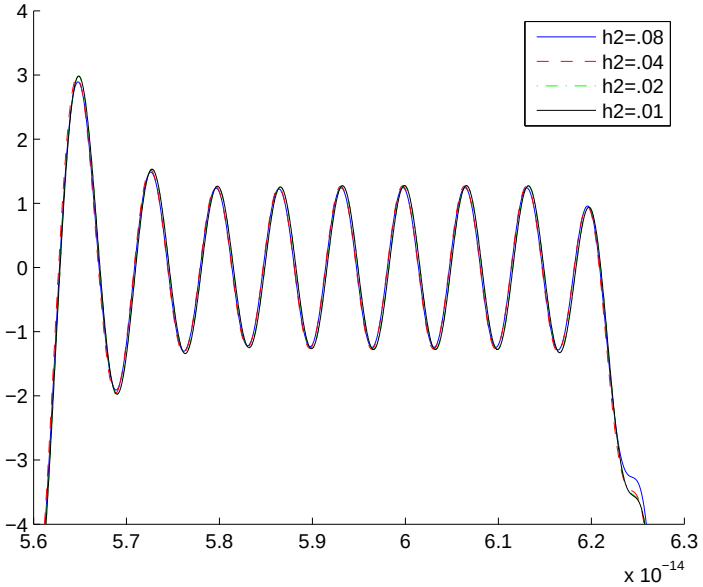

FIGURE 4.20: This plot shows the convergence of HOJHT. We have zoomed on the center of the curve for more detail.

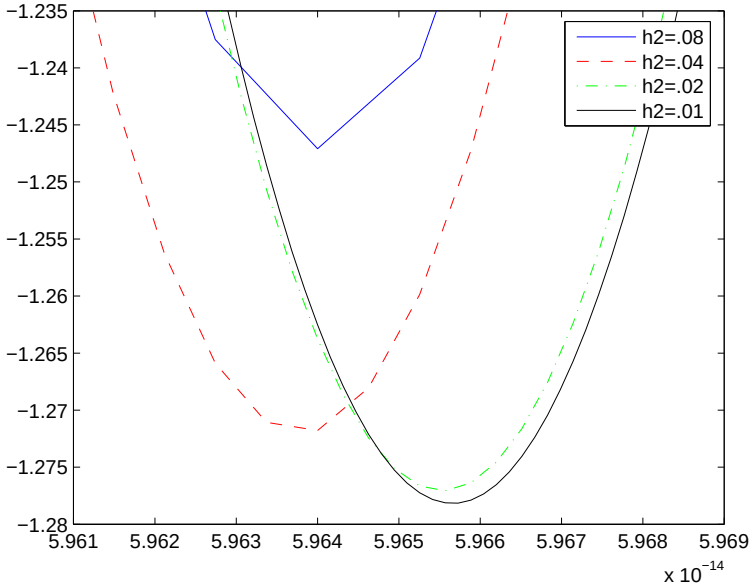

FIGURE 4.21: This plot shows the convergence of HOJHT. We have zoomed in on one of the center curves for more detail.

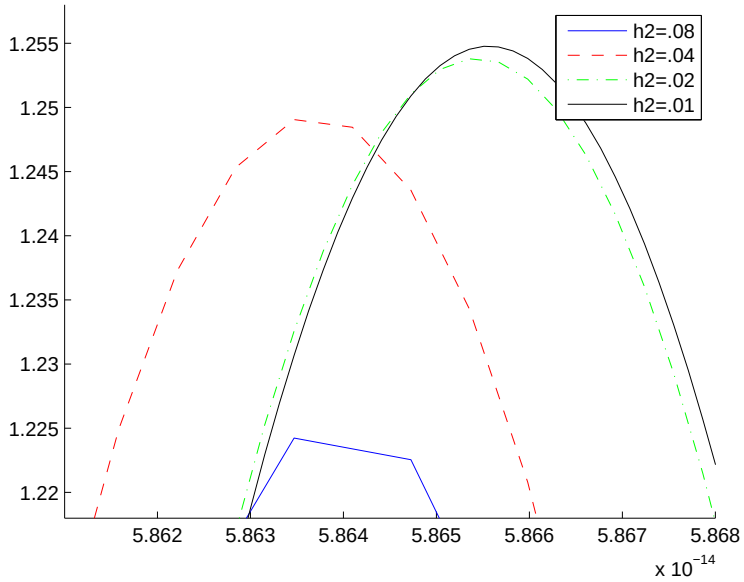

FIGURE 4.22: This plot shows the convergence of HOJHT. We have zoomed in on one of the center curves for more detail.

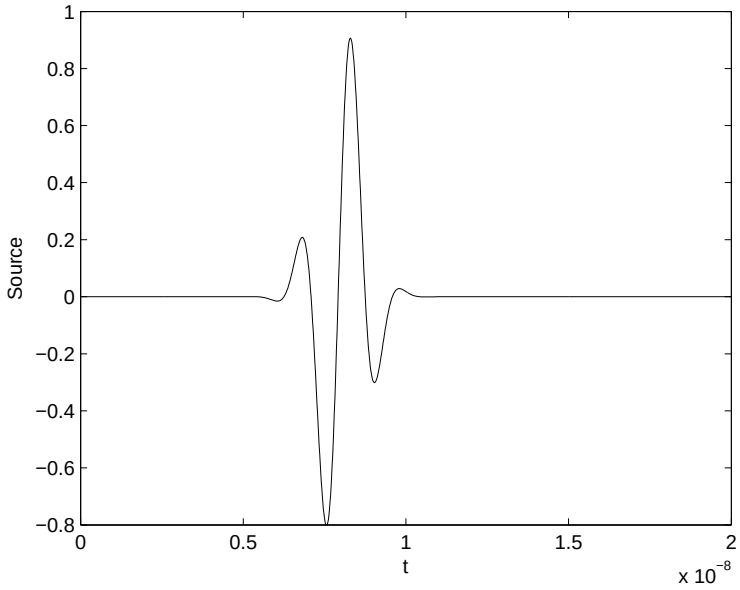

FIGURE 4.23: This plot shows the pulse used in the third simulation.

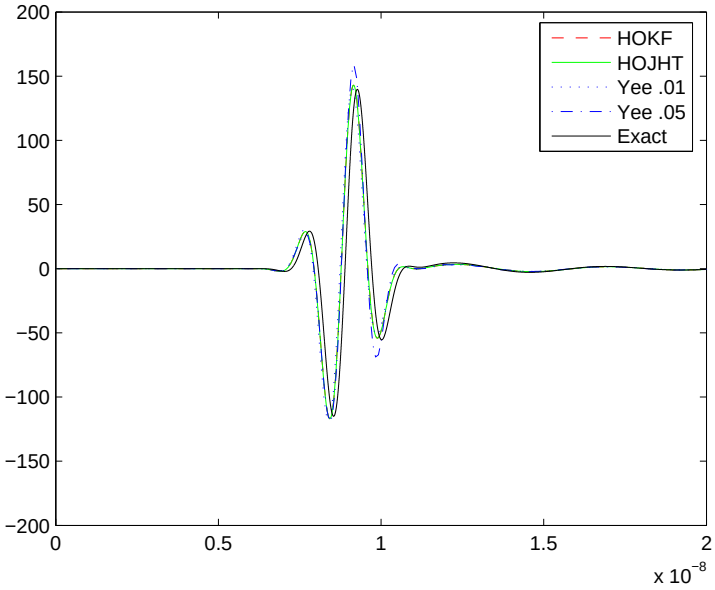

FIGURE 4.24: This plot shows Yee scheme plotted for $\Delta = .01$ and .05 as well as HOJHT and HOKF plotted with $\Delta = .05$.

5. CONCLUSION

In this paper, we compared fourth-order accurate in space schemes with second-order accurate schemes for Debye and Lorentz media simulations. Our stability plots show that a value of h_1=.01 is needed in order to manage dissipation in Lorentz media. This implies that $\Delta t \approx O(10^{-2}\tau)$. This result concurs with the results obtained in [11]. The HOKF scheme has less dissipation for wavenumbers k=$\left[0, 5 \times 10^8\right]$ for $h_1 = .1$ and behaves similarly for $h_1 = .01$ as compared to the KF scheme. The HOKF also performs better than the HOJHT scheme for $h_1 = .1$ because although it does have a little more dissipation, it does not become unstable for any values of $k\Delta$. The HOJHT scheme, along with the JHT scheme, both become unstable for some wavenumbers when $h_1 = .1$. This makes the HOJHT and JHT schemes unusable for those values of k. Similarly, our stability plots show that a value of $h_1 = 0.001$ is needed in order to manage dissipation in Debye media. This implies that $\Delta t \approx O(10^{-3}\tau)$ and also agrees with the results in [11]. As stated earlier, the higher-order schemes also have the advantage over the second-order schemes because of their ability to model stiff problems more effectively.

The HOKF and HOJHT schemes created less artificial dispersion than their second-order accurate counterparts in the vital domains of ω and $\omega\Delta t$. For example, in Figure 4.7 we see that the HOKF scheme has less artificial dispersion than the KF scheme for values of $\omega\Delta t$ up to approximately 1.9 for $h_1 = .1$. The value $\omega\Delta t = 1.9$ corresponds to about three points per period. The general rule is to use about 10 points per period or more. For values of 10 points per period or more, the HOKF scheme does indeed outperform the KF method. Also if we look at Figure 4.8 we see that the HOKF scheme has less artificial dispersion than the KF scheme for all values plotted. The same result can be seen for the HOJHT method. It displays less artificial dispersion than the JHT scheme for all values

of $\omega\Delta t$ and for ω. Where the HOKF scheme truly shines is in comparison to the HOJHT scheme in phase error analysis. For all values of $\omega\Delta t$ in Figure 4.11 and for all values of ω in Figure 4.12, the HOKF scheme shows much less artificial dispersion than the HOJHT method.

The simulations provide evidence to back the claims of Petropoulos [12] that higher order methods deal with stiff problems better by having the ability to reduce the value of ν without adding large amounts of dissipation. Also in the case of the first simulation, we see that the HOKF scheme converges faster and also has less dissipation for values of h_1 greater than .01.

Taking into account the stability and dispersion analysis as well as the simulations, it has been shown that using fourth-order accurate spatial derivatives does indeed improve the simulations of Maxwell's equations in dispersive media. It has also been shown that the HOKF scheme is a superior scheme based on the fact that it doesn't become unstable for any value of the wavenumber, k, it introduces less artificial dispersion than the HOJHT scheme and it shows less dissipation in the simulations.

BIBLIOGRAPHY

1. R. Albanese, R. Medina, and J. Penn, *Mathematics, medicine and microwaves*, Inverse Problems, 10 (1994), pp. 995–1007.

2. H. Banks and V. Bokil, *A computational and statistical framework for multidimensional domain acoustooptic material interrogation*, Quarterly of Applied Mathematics, 63 (2005), pp. 156–200.

3. H. Banks, V. Bokil, and N. Gibson, *Analysis of Stability and Dispersion in a Finite Element Method for Debye and Lorentz Dispersive Media*, to appear in Numerical Methods for Partial Differential Equations.

4. G. Cohen, *Higher-Order Numerical Methods for Transient Wave Equations*, Springer, 2002.

5. R. M. Joseph, S. C. Hagness, and A. Taflove, *Direct time integration of Maxwell's equations in linear dispersive media with absorption for scattering and propagation of femtosecond electromagnetic pulses*, Optics Lett., 16 (1991), pp. 1412–1414.

6. T. Kashiwa and I. Fukai, *A treatment by the FD-TD method of the dispersive characteristics associated with electronic polarization*, Microw. Opt. Technol. Lett, 3 (1990), pp. 203–205.

7. J. Lee, R. Lee, and A. Cangellaris, *Time-domain finite-element methods*, Antennas and Propagation, IEEE Transactions on, 45 (1997), pp. 430–442.

8. R. Lee and A. Cangellaris, *A study of discretization error in the finite element approximationof wave solutions*, Antennas and Propagation, IEEE Transactions on, 40 (1992), pp. 542–549.

9. P. Monk, *A Comparison of Three Mixed Methods for the Time-Dependent Maxwells Equations*, SIAM Journal on Scientific and Statistical Computing, 13 (1992), p. 1097.

10. A. Pereda, L. Vielva, A. Vegas, and A. Prieto, *Analyzing the stability of the FDTD technique by combining the vonNeumann method with the Routh-Hurwitz criterion*, Microwave Theory and Techniques, IEEE Transactions on, 49 (2001), pp. 377–381.

11. P. Petropoulos, *Stability and phase error analysis of FD-TD in dispersive dielectrics*, IEEE Trans. Antennas Propagat., 42 (1994), pp. 62–69.

12. P. Petropoulos, *The wave hierarchy for propagation in relaxing dielectrics*, Wave Motion, 21 (1995), pp. 253–262.

13. K. P. Prokopidis, E. P. Kosmidou, and T. D. Tsiboukis, *An fdtd algorithm for wave propagation is dispersive media using higher-order schemes*, J. Electromagnetic Waves Appl., 18 (2004), pp. 1171–1194.

14. A. Sihvola, *Electromagnetic Mixing Formulas and Applications*, Iet, 1999.

15. N. Stoykov, T. Kuiken, M. Lowery, and A. Taflove, *Finite-element time-domain algorithms for modeling linear Debye and Lorentz dielectric dispersions at low frequencies*, Biomedical Engineering, IEEE Transactions on, 50 (2003), pp. 1100–1107.

16. J. Strikwerda, *Finite Difference Schemes and Partial Differential Equations*, Society for Industrial Mathematics, 2004.

17. D. Sullivan, *Electromagnetic simulation using the FDTD method*, IEEE Press, New York, 2000.

18. A. Taflove, *Why study electromagnetics: the first unit in an undergraduate electromagnetics course*, Antennas and Propagation Magazine, IEEE, 44 (2002), pp. 132–139.

19. A. Taflove and S. C. Hagness, *Computational Electrodynamics: The Finite-Difference Time-Domain method*, Artech House, Norwood, MA, 3rd ed., 2005.

20. L. N. Trefethen, *Group velocity in finite difference schemes*, SIAM Review, 24 (1982), pp. 113–136.

21. K. Yee et al., *Numerical solution of initial boundary value problems involving Maxwells equations in isotropic media*, IEEE Trans. Antennas Propagat, 14 (1966), pp. 302–307.

22. A. Yefet and P. Petropoulos, *A Staggered Fourth-Order Accurate Explicit Finite Difference Scheme for the Time-Domain Maxwell's Equations*, J. Comput. Phys., 168 (2001), pp. 286–315.